NUMERICAL INVESTIGATIONS OF LATERAL JETS FOR MISSILE AERODYNAMICS

A THESIS SUBMITTED TO
THE GRADUATE SCHOOL OF NATURAL AND APPLIED SCIENCES
OF
MIDDLE EAST TECHNICAL UNIVERSITY

BY

EKİN AĞSARLIOĞLU

IN PARTIAL FULFILLMENT OF THE REQUIREMENTS
FOR
THE DEGREE OF MASTER OF SCIENCE
IN
MECHANICAL ENGINEERING

SEPTEMBER 2011

Approval of the thesis

NUMERICAL INVESTIGATIONS OF LATERAL JETS FOR MISSILE AERODYNAMICS

Submitted by **EKİN AĞSARLIOĞLU** in partial fulfillment of the requirements for the degree of **Master of Science in Mechanical Engineering Department, Middle East Technical University** by,

Prof. Dr. Canan ÖZGEN ________________
Dean, Graduate School of **Natural and Applied Sciences**

Prof. Dr. Süha ORAL ________________
Head of Department, **Mechanical Engineering**

Prof. Dr. Kahraman ALBAYRAK ________________
Supervisor, **Mechanical Engineering Dept., METU**

Examining Committee Members:

Prof. Dr. Mehmet Haluk AKSEL ________________
Mechanical Engineering Dept., METU

Prof. Dr. Kahraman ALBAYRAK ________________
Mechanical Engineering Dept., METU

Assist. Prof. Dr. Cüneyt SERT ________________
Mechanical Engineering Dept., METU

Assist. Prof. Dr. Mehmet Metin YAVUZ ________________
Mechanical Engineering Dept., METU

Ali AKGÜL, M.Sc. ________________
Chief Engineer, ROKETSAN

Date: 14/09/2011

I hereby declare that all the information in this document has been obtained and presented in accordance with academic rules and ethical conduct. I also declare that, as required by these rules and conduct, I have fully cited and referenced all material and results that are not original to this work.

Name, Last name : Ekin AĞSARLIOĞLU

Signature :

ABSTRACT

NUMERICAL INVESTIGATIONS OF LATERAL JETS FOR MISSILE AERODYNAMICS

Ağsarlıoğlu, Ekin
M.Sc., Department of Mechanical Engineering
Supervisor: Prof. Dr. Kahraman Albayrak

September 2011, 79 Pages

In this thesis, effects of sonic lateral jets on aerodynamics of missiles and missile-like geometries are investigated numerically by commercial Computational Fluid Dynamics (CFD) software FLUENT. The study consists of two parts. In the first part, two generic missile-like geometries with lateral jets, of which experimental data are available in literature, are analyzed by the software for validation studies. As the result of this study, experimental data and CFD results are in good agreement with each other in spite of some discrepancies. Also a turbulence model study is conducted by one of test models. It is also found out that k-ε turbulence model is the most suitable model for this kind of problems in terms of accuracy and ease of convergence. In the second part of the thesis, parametric studies are conducted on a generic supersonic missile, NASA TCM, to see the effect of jet parameters on missile and component force and moments in pitch plane. Variable parameters are jet location, jet mass flow rate and angle of attack. As a result, it was found out that downstream influence zone of jet exit is more than the upstream influence zone.

Normal force occurring by the interaction of the free stream and jet plume are amplified whenever the jet exit is located between lifting surfaces. Greater pitching moments are obtained when the jet exit moment arm with respect to moment reference center or jet mass flow rate is increased.

Keywords: Computational Fluid Dynamics, Supersonic Flow, Lateral Jet, Wind Tunnel Validation, FLUENT

ÖZ

YAN JETLERİN FÜZE AERODİNAMİĞİ AÇISINDAN SAYISAL OLARAK İNCELENMESİ

Ağsarlıoğlu, Ekin
Yüksek Lisans, Makina Mühendisliği Bölümü
Tez Yöneticisi: Prof. Dr. Kahraman Albayrak

Eylül 2011, 79 Sayfa

Bu tezde, ses hızındaki yan jetlerin ses üstü akış rejiminde uçan genel geçer füze ve benzeri geometriler üzerindeki aerodinamik etkileri, bir ticari hesaplamalı akışkanlar dinamiği yazılımı olan FLUENT ile sayısal olarak incelenmiştir. Çalışma iki bölümden oluşmaktadır. Birinci bölümde literatürde deney verileri olan iki denek taşı modeli, doğrulama çalışmaları kapsamında belirtilen programla analiz edilmiştir. Bu çalışma sonucunda deney verilerinin analiz sonuçları ile küçük farklılıklar dışında tutarlı olduğu gözlemlenmiştir. Ayrıca bir denek taşı modeli ile türbülans modeli çalışması yapılmıştır. Türbülans modeli çalışması sonucunda; k-ε türbülans modelinin, sonuçlara yakınlık ve yakınsama kolaylığı açısından böyle bir akış problemi için kullanılmasının uygun olduğu saptanmıştır. Tezin ikinci bölümünde, NASA TCM isimli genel geçer ses üstü füzesi üzerinde, çeşitli jet özelliklerinin yunuslama düzleminde füze ve bileşenleri üzerine etkiyen kuvvet ve momentler üzerindeki etkilerni incelemek için parametrik bir çalışma yapılmıştır. Bu çalışmada değişkenler; jet konumu, jet debisi ve hücum açısı olarak belirlenmiştir. İkinci kısımda yapılan çalışma sonucunda, jet etkilerinin akış altı bölgesinde, akış üstü bölgesine göre daha fazla alanda etkin olduğu saptanmıştır. Jet çıkışı ve serbest akış etkileşimi ile ortaya çıkan normal kuvvetin; jetin etrafında kanat veya kuyruk gibi bir yüzey olması durumunda arttığı belirlenmiştir. Jet çıkşının moment referans merkezinden uzaklaşması veya jet debisinin artması ile füzeye etki eden toplam yunuslama momentinin arttığı kaydedilmiştir.

Anahtar Kelimeler: Hesaplamalı Akışkanlar Dinamiği, Ses Üstü Akış, Yan Jet, Rüzgar Tüneli, FLUENT

To My Parents

ACKNOWLEDGEMENTS

I wish my deepest gratitude to my supervisor Prof. Dr. Kahraman Albayrak for his guidance, advice, criticism and encouragements throughout the thesis.

I also wish to thank my chief engineer Mr. Ali Akgül for his guidance and support during this study. I also would like to thank my colleagues in Aerodynamics Division of ROKETSAN for all their help and support during the thesis.

I am very thankful to my parents Mrs. Safiye Ağsarlıoğlu and Mr. Ali Hamdi Ağsarlıoğlu for their help and motivation. Without then this work would not be completed.

The last but not the least, I want to express my best wishes to Ms. Senem Karakaya, Mr. Murat Ekşi and Mr. Mehmet Akgül for their friendship and support during this study.

TABLE OF CONTENTS

LIST OF FIGURES

FIGURES

LIST OF TABLES

TABLES

LIST OF SYMBOLS

SYMBOLS

C_A	: Axial force coefficient
C_N	: Normal force coefficient
C_Y	: Side force coefficient
C_l	: Rolling moment coefficient
C_m	: Pitching moment coefficient
C_n	: Yawing moment coefficient
x, y, z	: Body axis coordinates
$C.G.$	: Center of gravity
α	: Angle of attack
δ	: Pitch (elevator) deflection
ρ	: Density
p	: Pressure
T	: Temperature
V	: Velocity
μ	: Dynamic viscosity
h	: Enthalpy
R	: Gas constant
S	: Sutherland constant
τ_{ij}'	: Viscous stress tensor
e	: Internal energy
M	: Mach number
F	: Force
A	: Area
$\dot{m}$	: Mass flow rate
k	: Ratio of specific heats

q	: Dynamic pressure
Φ	: Arbitrary scalar in conservation equation
Γ	: Diffusive coefficient
u_i	: i^{th} component of velocity vector
μ_t	: Turbulent viscosity
k	: Turbulent kinetic energy for turbulence
ε	: Turbulent dissipation rate
u_τ	: Friction velocity
C_f	: Skin friction coefficient
ν	: Kinematic viscosity
Re	: Reynolds number
y^+	: Cell wall distance parameter
U	: Free stream velocity
K	: Force amplification factor
X_{CPi}	: Interaction moment center
TCM	: Tandem control missile
Ci	: i^{th} TCM configuration depending on jet location

Subscripts

jet	: Jet properties
jet,on	: Active jet phase
jet,off	: Passive jet phase
∞, *amb*	: Free stream properties
mc	: Moment center
Ci	: i^{th} canard
Ti	: i^{th} tail
REST	: Total missile configuration excluding jet exit
s	: Static properties
0	: Stagnation properties

CHAPTER 1

INTRODUCTION

Missiles unless they have ballistic trajectories, need some kind of a control mechanism for maneuvering. Changing the trajectory of a missile is done by imposing additional aerodynamic forces on the missile. For a six degree of freedom and body fixed coordinate system, aerodynamic force and moment coefficients are shown in Figure 1-1.

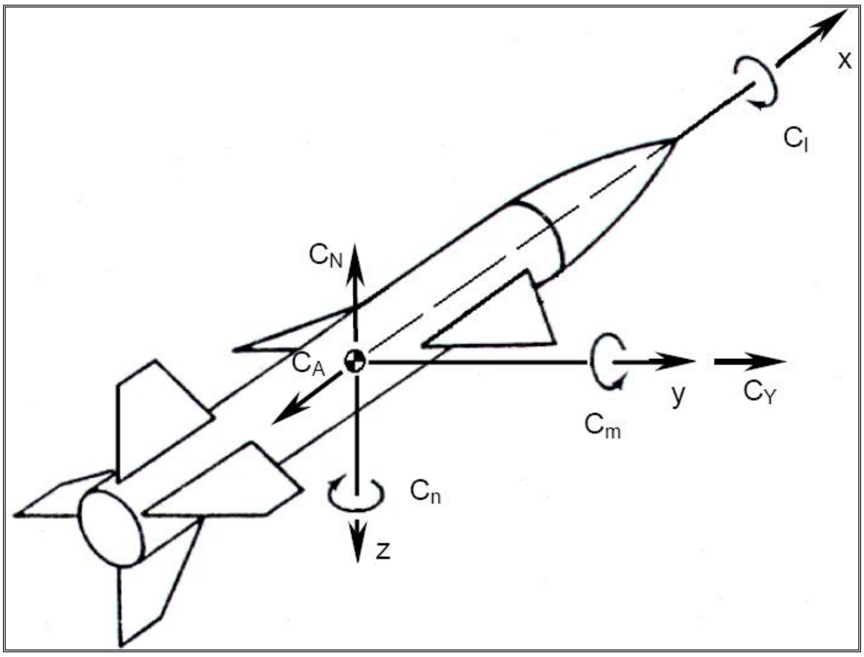

Figure 1-1: Forces and Moments Acting on a Missile

In the above figure, C_A is the axial force coefficient. Moment coefficient about x-axis is C_l and it is called the rolling moment. Coefficients for normal and side forces are C_N and C_Y respectively. Pitching moment coefficient is C_m and yawing moment coefficient is C_n. All the mentioned parameters are calculated by dividing the forces and moments by free stream dynamic pressure, reference area and length (for moments). "*x-z*" plane is the pitch plane and "*x-y*" plane is the yaw plane for a body-fixed coordinate system. For the motion in pitch plane, axial force, normal force and pitching moment coefficients are used for motion equation in flight simulations.

Aerodynamic axial force on the missile is balanced with the thrust of the missile when there is no acceleration. For changing the trajectory of the missile in body fixed coordinate system in pitch plane, i.e. maneuvering, normal force and/or pitching moment acting on the missile should be non zero. When a normal force acts on a missile on a location other than the center of gravity, pitching moment is also generated and missile translates and rotates at the same time. When the normal force acts on the center of gravity, only translational motion occurs. Forces and moments are imposed on the missile in two ways generally, which are defined below.

1.1 Conventional Control Systems

Conventional control systems consist of deflecting lifting surfaces located on the body of the missile. This type of control is also called aerodynamic control. Two types may be named generally. Canard control type and tail control type are two most common types. In Figure 1-2 and Figure 1-3, these control system types can be seen schematically [1].

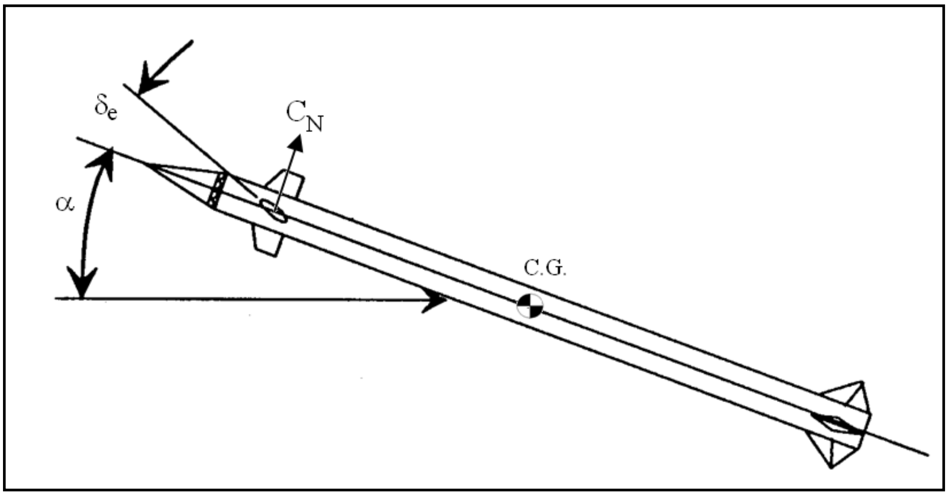

Figure 1-2: Conventional Control Systems, Canard Control [1]

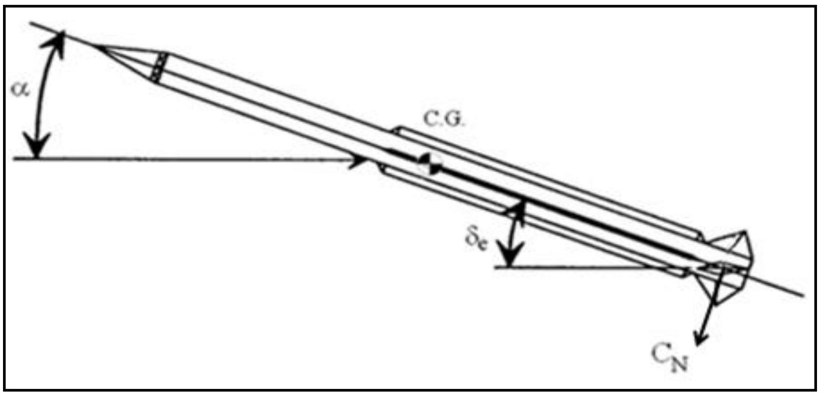

Figure 1-3: Conventional Control Systems, Tail Control [1]

In the above figure, α is the angle of attack. As it may be observed from the above pictures, the deflected control surfaces create normal forces, thus pitching moments with respect to center of gravity of the missile. This moment results in a maneuver about the pitch axis of the missile.

Deflection of these control surfaces is done by actuating systems. These systems consist of electric/pneumatic/hydraulic motors and control input is given by the autopilot or manually, depending on the subsystem of the missile.

1.2 Alternative Control Techniques

Other than control surface deflection, reaction type control systems have recently been used in the missiles. In this type; instead of a deflecting lifting surface, high speed ejecting fluid or thrust deflection techniques are used to create a maneuvering force. Alternative control systems are also called reaction type control systems. Two main types are thrust vector control systems (TVC) and side-jet control systems.

TVC systems use the principle of thrust deflection to get pitching or yawing moments for maneuvering. Figure 1-4 shows a schematic of a TVC system [2].

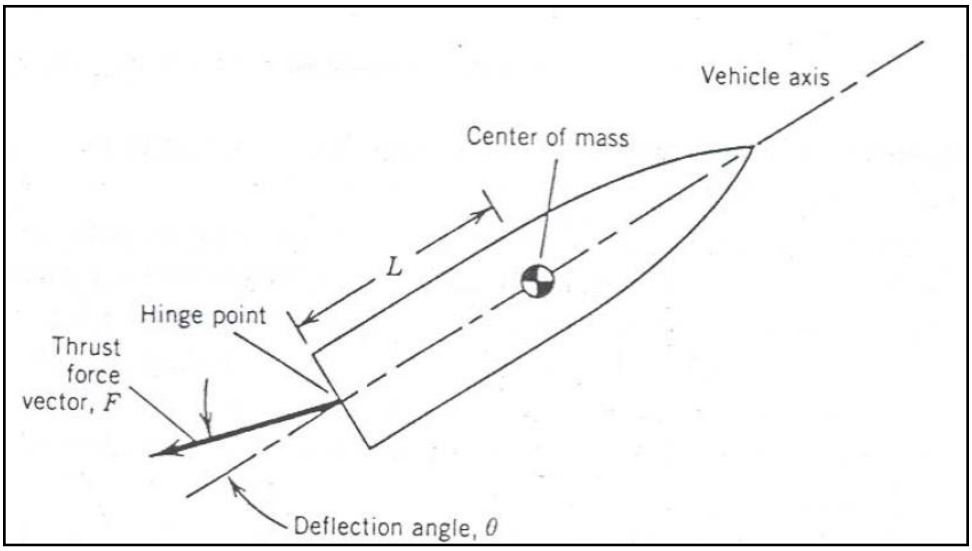

Figure 1-4: Thrust Vector Control System [2]

It is clear from the above figure that force and moment necessary for turning maneuvers are supplied to the projectile by deflecting the direction of plume which supplies the thrust force. Normal component of the thrust force creates the pitching moment like the deflected lifting surfaces in conventional control surfaces.

Thrust vector controlling may be applied by various ways [2]. Movable nozzles may be inserted into the exit of the rocket motor so that the thrust can be deflected. Jet vanes also may be used for thrust deflection. Secondary gas injection may be used for distorting the exhaust gas flow to obtain a normal force component. Auxiliary thrust chambers are used as another option for thrust vector controlling.

Besides thrust vector controlling, lateral jets, or sometimes called side-jets are used as reaction type control systems. High pressure jets are ejected into free stream in normal direction and they create forces and moments for maneuvering. In Figure 1-5, there is a schematic representation of side-jets [3]

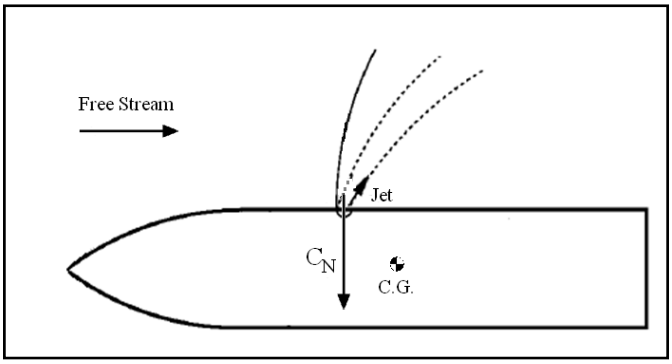

Figure 1-5: Side-Jet Schematic [3]

It is clear from the above figure that the ejection of jet in upward direction causes a downward force from the fluid to the projectile and this force creates pitching moment about center of gravity for maneuvering, as the flow is considered in *x-z* plane according to Figure 1-1. Interaction of the jet with the free stream results in a highly complicated flow field [4]. Features and details of the complicated flow field are discussed in upcoming chapters.

1.3 Lateral Jet Systems in General

Lateral jet controls systems are being considered as attractive alternatives to conventional surface control systems in recent years [5].There are some advantages of these systems to conventional control surfaces.

- In low dynamic pressures, i.e. high altitude or low speed flight, conventional control surfaces lose their control effectiveness. Side-jet control systems are highly effective in high altitude, low density regions.
- Side-jet control results in faster response for maneuvering. Conventional control systems always contain a larger lag in control input and system response than reaction type control systems.
- In addition to rapid reaction, greater control force can be obtained from side-jets. Increasing the jet pressure or mass flow rate of the jet increases the momentum transfer to the missile.
- Missiles with conventional control surfaces have stall problem at high angles of attack. Stalling results in flow separation and loss of control effectiveness for lifting surfaces [6]. Thus control surface deflection angle and angle of attack for the projectile are limited to some extent. But side-jet controlled missiles do not have a stall problem so that they can provide higher angles of attack to the missile.

Lateral-jet systems also have disadvantages compared to control surfaces. Major disadvantages are:

- This type of control systems are generally used in missiles travelling in supersonic Mach numbers. The interaction of the ejected gas with supersonic free stream results in highly complicated flow field [7]. There are shock-boundary layer interactions, expansions etc. that affect the external aerodynamics very much. In Figure 1-6, there is a schematic representation of the resulting flow field.
- Since the resulting flow field is very complex and this changes the external aerodynamics of the projectile, the flow field has to be analyzed carefully. Deciding upon the jet parameters are very important and very good prediction of the aerodynamic effects of interaction on full missile configuration is a must.

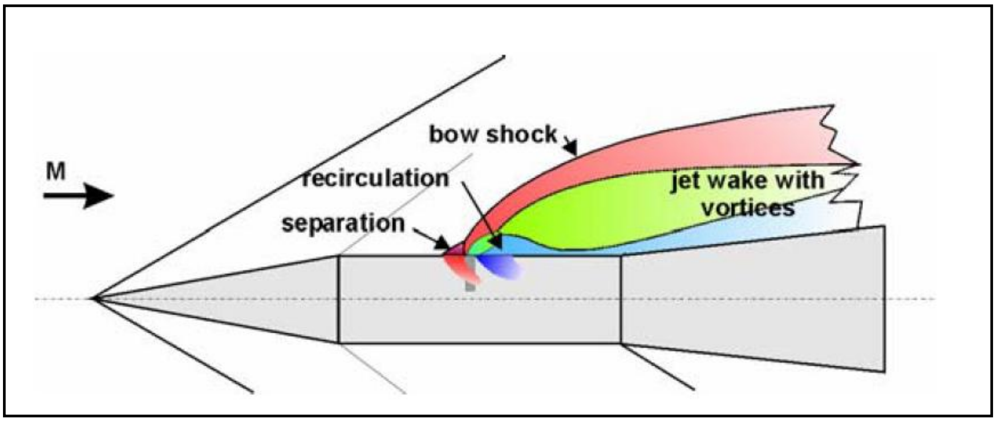

Figure 1-6: Schematic Representation of the Resulting Flow Field [7]

In industry, there are missiles designed with lateral jet control systems alone or a control system with a combination of lateral jet and another system. Main examples of these missiles are:

- LOSAT (Line of Sight Anti Tank Weapon)[1] [8]: Designed and produced by Lockheed Martin, this missile used only lateral jet system for steering purposes. It is a medium range, supersonic anti tank missile. The production of the missile is terminated after 435 units. Picture of this missile during firing can be viewed in Figure 1-7.

Figure 1-7: LOSAT Missile [8]

- THAAD (Terminal High Altitude Area Defense) [1][9][10]: This is another missile designed and produced by Lockheed Martin. Main objective of this missile is the interception of enemy missiles and it is used as an air defense weapon. Operation regime is hypersonic. Side jets are used in combination with the movable nozzle mechanism for steering purposes. In Figure 1-8, THAAD missile may be seen.

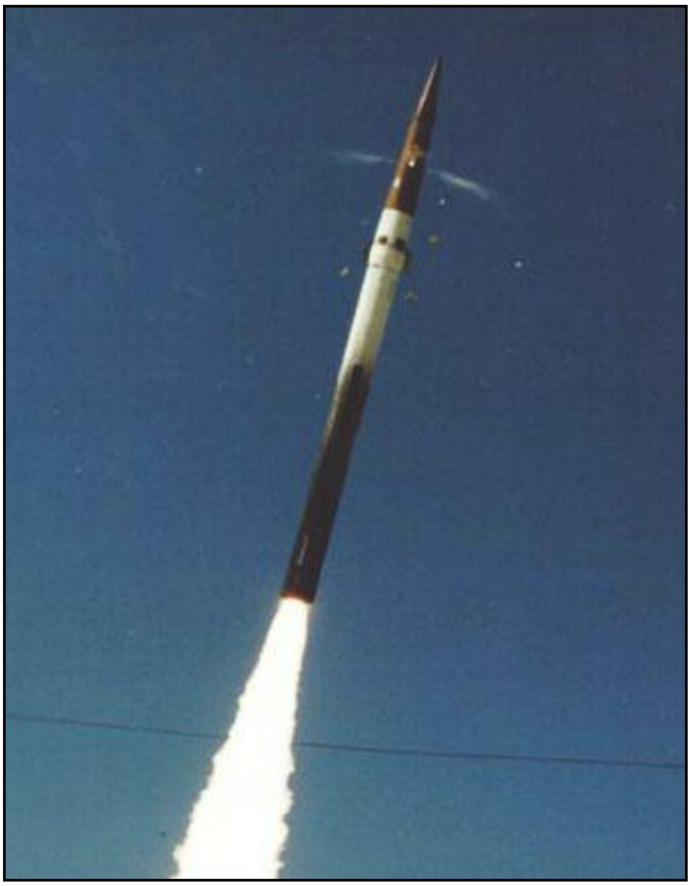

Figure 1-8: THAAD Missile [9]

- PAC-3 (Patriot Advanced Capability-3) [1][11][12]: Hypersonic long range air defense missile. This missile uses the combination of conventional aerodynamic control with side jets. In Figure 1-9, PAC-3 missile is shown.

Figure 1-9: PAC-3 Missile [11]

This type of control systems are generally used in homing or launch phase of the missile, when the high maneuverability is required. Lateral jet control systems have a highly pressurized gas chamber located in missile body in axial direction. Injected fluid may be air, nitrogen [13] or some other gas. Injected fluid is generally selected air or nitrogen mixtures because mixing or reacting injected fluid add more complexity to the problem and further affect the flow field.

Main parameters in the lateral jet controlled systems are jet location, jet pressure, jet mass flow rate and missile configuration. Options are the choice of the designer. For example, in order to get higher control forces, injected gas pressure is increased. If larger pitching moment is necessary, jet is located further away from the center of gravity. If the designer does not want to distort the base flow, jet is placed at the front part of the missile.

1.4 Lateral Jet in Literature and Aim of This Thesis

From 1960's to nowadays, projectiles with lateral cross-jets are under research analytically, experimentally and numerically. Earlier studies by Orth and Funk [13] investigated the transonic and supersonic jet injection to the flat plate for different injected fluids and determined the injected fluid penetration. Schetz [15] researched both liquid and gaseous injectants analytically and compared the results with the experiments. Werle et.al. [16] conducted series of high supersonic free stream flat plate jet injection experiments and tried to develop correlations by analyzing the surface pressure recordings and geometric shock properties from shadowgraphs.

Brandeis and Gill [14] considered five different generic missile configurations and conducted both jet-on and jet-off experiments for different free stream Mach numbers and different angles of attack. By analyzing force and moment values for both situations, they investigated the force amplification and center of pressure shift in the presence of jet. Graham and Weinacht [3] investigated Brandeis and Gill's work by a numerical Reynolds Averaged Navier-Stokes code and compared the surface pressure distribution for different configurations with experimental data. Srivastava [5] investigated the jet interaction effects for a generic supersonic missile body by a numerical RANS code and compared the force and moment values for both jet-on and jet-off conditions. His research also included different wing geometries, jet location and angle of attack effects. He also compared the results with the wind tunnel data and the numerical results were in good agreement with experiments. Gnemmi and Adeli [7] also did numerical RANS calculations with commercial software on a generic supersonic missile body and compared surface pressure distributions for different azimuth angles with experimental data. Lee et.al. [17] did numerical RANS calculations and formed a force and moment coefficient database for flight simulations. Higgins et.al. [18] used a hybrid RANS-LES code for a jet injection from a flat plate to make comparisons with RANS codes and experiments. Schülein [19] did comparative studies of jet injection on a flat plate. Recently, DeSpirito [20] computationally investigated the effects of jet location on a generic supersonic missile. The study consists of the effects of jet location, pressure and temperature on force and moment amplification.

The aim of this study is to clearly identify the complex flow physics resulting from the interaction of supersonic free stream and side-jet. Validation studies will be presented using two test models from the literature [7], [13], using a commercial CFD software FLUENT®. After validating the numerical tools for lateral jet controlled missile problems, jet effects on a generic missile body, NASA-TCM [21], for different jet parameters such as angle of attack, jet pressure ratio and jet location will be investigated.

CHAPTER 2

METHODOLOGY

In this part, firstly the governing equations concerning the fluid flow of a supersonic missile with lateral jet control will be mentioned. After introduction of the governing equations, details of the resulting flow field will be given. Finally discretization techniques used in this study will be given and numerical tools will be introduced.

2.1 Governing Equations

Governing equations concerned with the problem mentioned in this study are firstly three fundamental conservation laws, which are conservation of mass, momentum and energy. They are given in three dimensions in differential form sequentially below [22].

$$\frac{\partial \rho}{\partial t} + \mathrm{div}\rho\mathrm{V} = 0 \tag{2.1}$$

$$\rho \frac{D\mathrm{V}}{Dt} = \rho \mathrm{g} + \nabla \cdot \tau_{ij}{}' + \nabla \mathrm{p} \tag{2.2}$$

$$\rho \frac{Dh}{Dt} = \frac{Dp}{Dt} + \mathrm{div}(k\nabla T) + \tau_{ij}{}' \frac{\partial u_i}{\partial x_j} \tag{2.3}$$

Where τ_{ij}' is the viscous stress tensor for a Newtonian fluid and it is defined below.

$$\tau_{ij}' = \mu\left(\frac{\partial u_i}{\partial x_j} + \frac{\partial u_j}{\partial x_i}\right) + \delta_{ij}\lambda\,\mathrm{divV} \tag{2.4}$$

In the derivation of conservation equations, infinitesimal control volume of fluid is selected and mass, momentum and energy balance is done for the faces of the element. Detailed derivations of these equations may be found in textbooks [22]. In these equations there are seven unknown variables. Three primary variables, which have to be obtained simultaneously from the governing equations, are pressure (*p*), temperature (*T*) and velocity vector (*V*). Other remaining variables *ρ, μ, h* and *k* are derived from auxiliary relations or for some types of flow, they are assumed constant. Since compressible flow is concerned in this study, they are not assumed constant for everywhere in the flow. Fluids in flow are assumed to obey ideal gas law thus density is calculated from:

$$p = \rho RT \tag{2.5}$$

There are several options for calculating the dynamic viscosity term. Viscosity is mainly a function of operating temperature. The main options for calculating the viscosity term are linear, polynomial or power series approximations and Sutherland's law [23]. Three coefficient form of Sutherland's viscosity law is stated below.

$$\mu = \mu_0\left(\frac{T}{T_0}\right)^{3/2}\frac{T_0 + S}{T + S} \tag{2.6}$$

Where μ_0 is the reference dynamic viscosity, T is the ambient static temperature, S is the Sutherland constant in Kelvin and T_0 is the reference temperature. The remaining two variables to be calculated in the governing equations are fluid enthalpy h and thermal conductivity k. The fluid enthalpy is used to replace the internal energy per unit mass e in the derivation of the energy equation.

$$h = e + \frac{p}{\rho} \tag{2.7}$$

Like in viscosity, there are options for calculating the thermal conductivity k. It may be specified constant; or it may be defined by either a linear or polynomial approximation function dependent on temperature [23].

In addition to conservation equations, additional equations concerning the compressible fluid flow are also used in this study. These equations are used for calculating the stagnation state properties, such as temperature and pressure. T_0 and p_0 are defined as the pressure and temperature of a fluid particle in a flow which is brought to rest isentropically and adiabatically. The relations for these properties are given below [24].

$$\frac{p_0}{p} = \left(1 + \frac{k-1}{2} M^2\right)^{\frac{k}{k-1}} \tag{2.8}$$

$$\frac{T_0}{T} = 1 + \frac{k-1}{2} M^2 \tag{2.9}$$

Need for another equation arises when one wants to calculate the jet force produced by the jet alone. The force produced by the jet alone will be used in upcoming chapters. If the jet ejection is assumed perfectly –*z* direction in Figure 1-1, the net force produced on the missile body in *z* direction is calculated and non-dimensionalized as follows, similar to calculating rocket thrust [25]. Subscript *jet* is used for jet properties, *amb* for ambient and *e* for exit.

$$F_{jet} = \dot{m}_e V_e + A_e (p_e - p_{amb}) \tag{2.10}$$

$$C_{N,jet} = \frac{F_{jet}}{qS_{ref}} \tag{2.11}$$

2.2 Flow Features of Interaction of Supersonic Stream and Ejecting Jet

Flow field, resulting from the interaction of supersonic free stream and transverse jet is very complicated. In this section, some definitive features of the interaction flow field will be mentioned. It is better to first analyze this situation in a 2-D problem. In Figure 2-1, an idealized scheme of 2-D problem is shown [4].

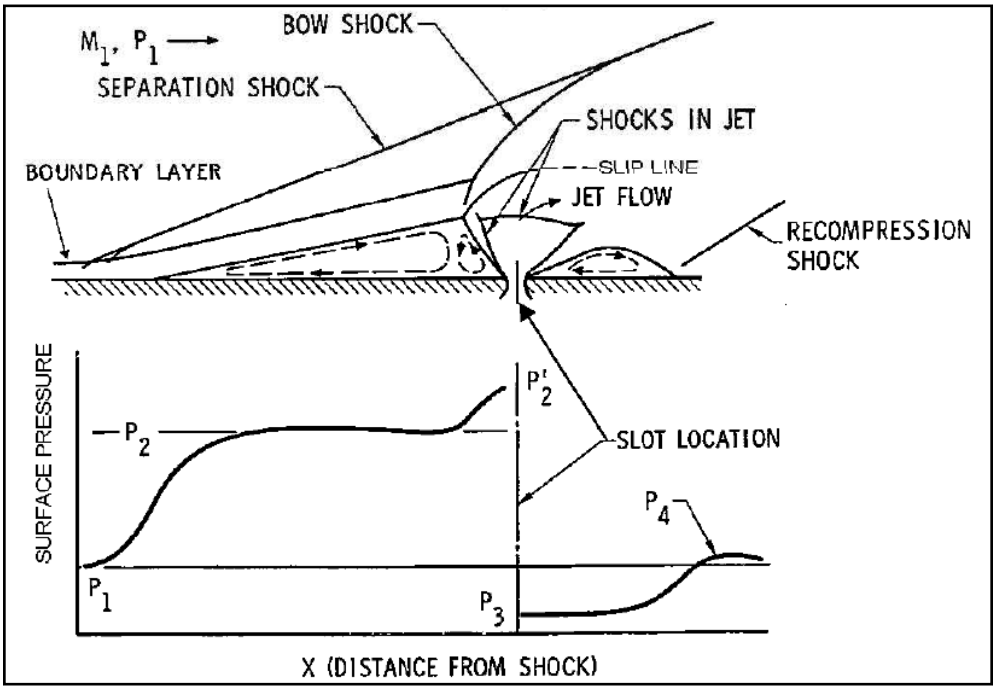

Figure 2-1: Schematic View of Jet Ejection through Infinite Span Flat Plate [4]

In this case, the supersonic flow is parallel over an infinite span flat plate. Jet slot also has infinite span. In the above picture the free stream – jet interaction flow field and surface static pressure distribution are shown. The main features of the flow are:

- The jet plume acts like an obstacle to the supersonic cross flow. A separated boundary layer forms in the vicinity of the jet exit.
- Separation shock forms near the separation line upstream of the jet plume.

- Due to jet being like an obstacle to the flow, a bow shock is formed near the jet plume.
- Separation shock meets the bow shock through the jet plume and two shocks form a mixing region.
- Ejecting jet expands very quickly and has very high velocity. Jet expansion waves form through the plume in order to decrease jet pressure.
- Another separation region is formed in the wake region. In this region pressure and velocity is lower than the upstream conditions. A recompression shock is formed in this region in order to accelerate the wake flow to free stream conditions.
- If surface pressure distribution is examined in the vicinity of the jet exit, pressure is higher than free stream pressure upstream of the jet and lower than free stream pressure downstream of the jet. This pressure difference causes a moment couple on the flat plate centered at the jet exit.

Flow visualization experiments were carried out by various scientists for jet interaction problems in the past. In Figure 2-2, there is a shadowgraph of a flow over a flat plate at a free stream Mach number of 2.61, with jet ejection. Bow shock and separation shock is clearly seen in Figure 2-2 [26].

Figure 2-2: 2-D Flat Plate with Jet Injection Shadowgraph [26]

The jet ejecting upwards creates a downward force on the flat plate due to conservation of momentum principle. But in order to understand the overall effect of the jet on the model, surface static pressure distribution upstream and downstream of the jet also has to be considered. Jet blockage effect causes a high pressure zone upstream and a low pressure zone downstream. The strengths of these zones may have favorable or adverse affects on normal force produced by the jet, depending on jet exit parameters.

In this thesis, jet effects over a missile are investigated so that 3-D effects should also be taken into account. In Figure 2-3, supersonic flow over a generic projectile body with a transverse jet is schematically represented [4].

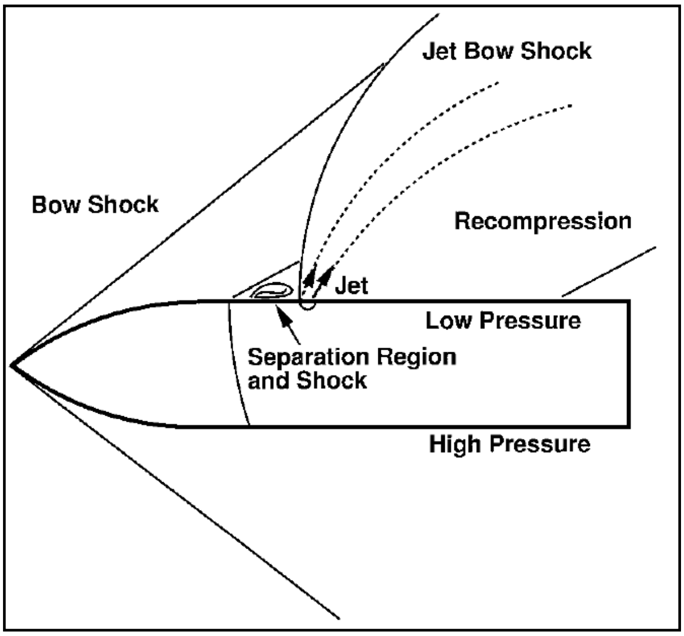

Figure 2-3: 3-D Jet Ejection Flow Physics Scheme over a Generic Projectile [4]

3-D flow over a jet injecting projectile is similar to the flat plate case, but there are some differences. Figure 2-3 shows the flow structure in *x-z* plane. Main flow features in this case are:

- Jet bow shock, separated region and separation shock and recompression region are also present in this case. In addition to these, there is a bow shock attached to the nose of the projectile. The mixing region in this case is between the nose bow shock and the jet bow shock. Nose bow shock is more dominant.
- The shock structure formed by the interaction is 3-D in this case. The shock structure is bounded and turned by the mixing layer in circumferential direction. The mixing layer surrounds the jet plume

upstream. High pressure region upstream and low pressure downstream are spread around the missile body, thus affecting the surface pressure distributions compared to no-jet case.

- Upper surface of the missile is highly affected by the jet ejection whereas the lower surface shows a typical supersonic stream pressure distribution. Upper downstream region of the missile has low pressure due to separation but the lower region has higher pressure. The pressure difference creates a vertical normal force opposite to the force created by the jet alone. In this type of flow, force created by the jet alone may be de-amplified by additional force resulting from pressure distribution.

Some experimental investigations are already present in the literature for lateral jet controlled projectile models, as discussed in the first chapter. In Figure 2-4, a shadowgraph a projectile with jet ejection may be seen [27]. The figure is showing the projectile in *x-z* plane and free stream Mach number is 2 in this case.

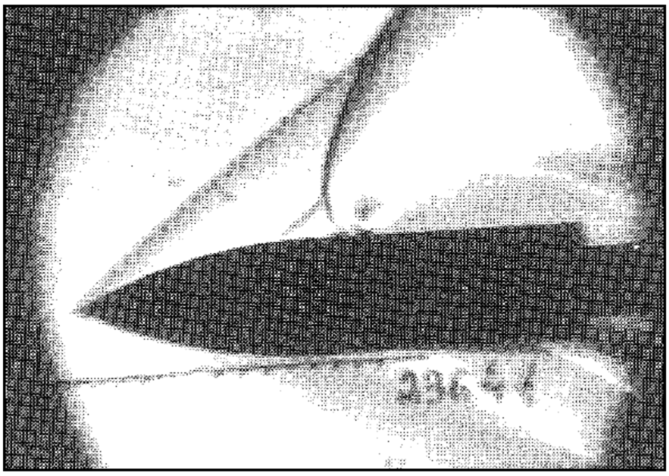

Figure 2-4: Shadowgraph of a Projectile Model with Lateral Jet [27]

Nose bow shock, upstream separation region, mixing region, upstream separation shock, recirculation region and recirculation shock are all present in this picture. Oil flow visualization of a projectile with jet ejection from *x-y* view is shown in Figure 2-5. In this picture, 3-D wraparound effect of shock structure is clearly seen. In addition to flat plate, jet effects spread in circumferential direction as the distance from the jet exit increases in *x* direction.

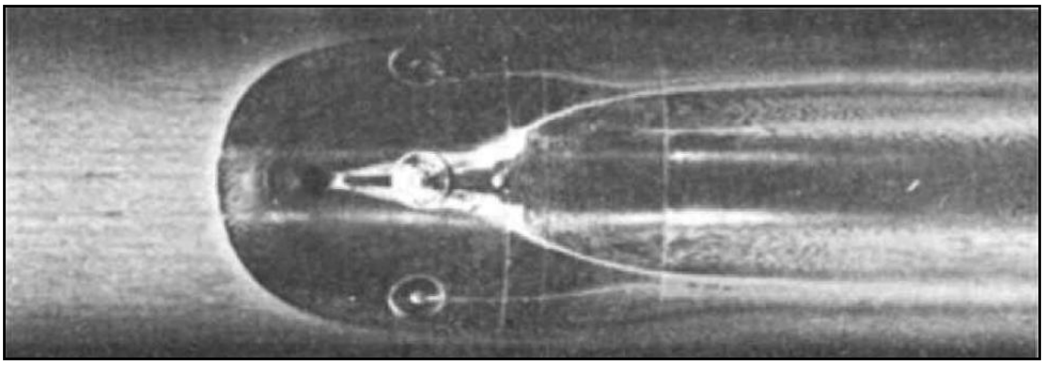

Figure 2-5: Oil flow of Top View of a Side Jet Controlled Projectile [4]

As it is clearly seen from the above schematics and experimental figures, flow structure over side jet controlled missiles is different from the conventionally controlled missile flow structures. The vicinity of the jet contains additional separation and shock regions, the jet itself also acts like an obstacle to the flow and affects upstream and downstream regions. As it may be observed, flow structure over a missile containing lateral jet is quite more complicated than flow structure over a conventionally controlled missile.

2.3 Numerical Tools and Equation Discretization

Governing equations of fluid motion are highly nonlinear equations and exact solutions of these equations exist for very special cases [22]. For a problem concerning the flow over a missile containing a lateral jet, a numerical approach is used for obtaining forces, moments, pressure distributions etc.

Numerical solver used in this study, FLUENT®, is Computational Fluid Dynamics (CFD) software which solves the conservation equations numerically with a finite volume approach [23]. Also this kind of a problem contains turbulence in its nature inevitably. In this part, a general overview of numerical approaches to be used in this study will be given.

For numerical solution, 3-D test case models and parametric study missile model flow domains will be meshed. A computational domain will be created for these models. Surface grids for missile models will be created in Gambit®, boundary layer grid will be created by TGrid®, and volume grid will be created in Gambit® again. Volume grid file will be exported to FLUENT® in .msh format. Surface grid will consist of triangular elements, boundary layer cells will be of wedge type and volume grid will contain tetrahedral elements. In Figure 2-6, grid generation and solution procedure is shown.

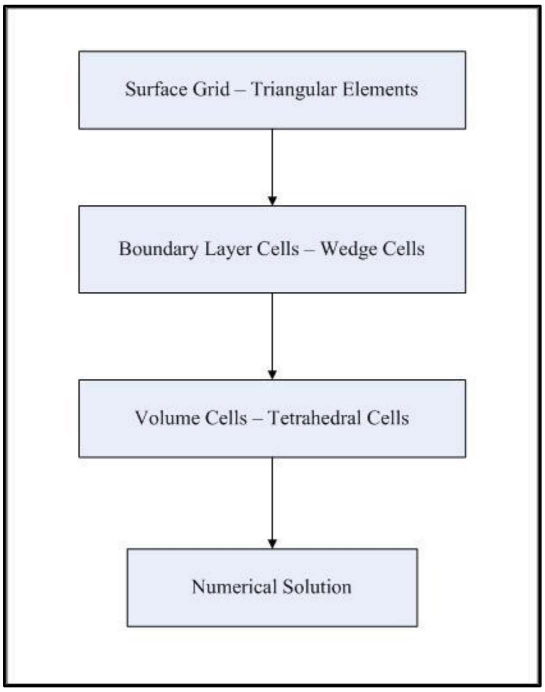

Figure 2-6: Grid Generation and Solution Sequence

For all problems, FLUENT solves the discretized form of continuity and momentum equations. Solving energy or species equations is optional to the user. FLUENT uses a finite-volume based approach to convert the general transport equation to a numerical equation. Unsteady conservation equation for an arbitrary scalar Φ in an arbitrary control volume V is:

$$\int_V \frac{\partial \rho \Phi}{\partial t} dV + \oint \rho \Phi \vec{V} \cdot d\vec{A} = \oint \Gamma_\Phi \nabla \Phi \cdot d\vec{A} + \int_V S_\Phi dV \qquad (2.12)$$

In the equation 2-12, Γ_Φ is the diffusive coefficient for Φ, and S_Φ is the source term. The above equation may be interpreted as the Φ stored in a control volume V is equal to the source term and differences between the diffusive and convective fluxes. Transport equation in the integral form is discretized as:

$$\frac{\partial \rho \Phi}{\partial t} V + \sum_{f}^{N_{faces}} \rho_f \vec{V}_f \Phi_f \cdot \vec{A}_f = \sum_{f}^{N_{faces}} \Gamma_\Phi \nabla \Phi_f \cdot \vec{A}_f + S_\Phi V \tag{2.13}$$

Where N_{faces} is the number of faces enclosing the cell, Φ_f is the value of Φ convected through the face, $\rho_f \vec{V}_f \cdot \vec{A}_f$ is the mass flux through the face. Schematically these variables are shown in Figure 2-7 below. In the figure, c_0 and c_1 denote the cell number, f is the face centroid.

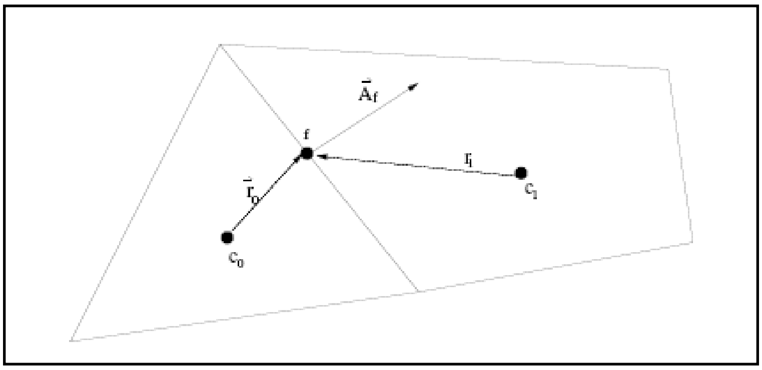

Figure 2-7: 2-D Representation of Two Control Volumes and Parameters in Discretized Equation [23]

In FLUENT, there are two options for the solver type. First choice is the density based solver and second choice is the pressure base solver. Pressure based solver is developed for low speed incompressible flows, density based solver is developed for high speed compressible flows at first. But due to improvements in the software and addition of some extra options in the latest versions, both solvers may be used for other regimes than their first intents.

Major difference between the solvers is; in pressure based solver, whether it is segregated or coupled, conservation equations are not solved simultaneously with each other. Conservation equations are coupled with each other in the density based solver. Since governing equations are solved at the same time in the coupled solver, instantaneous memory demand is higher. Density based solver sequence is given in Figure 2-8.

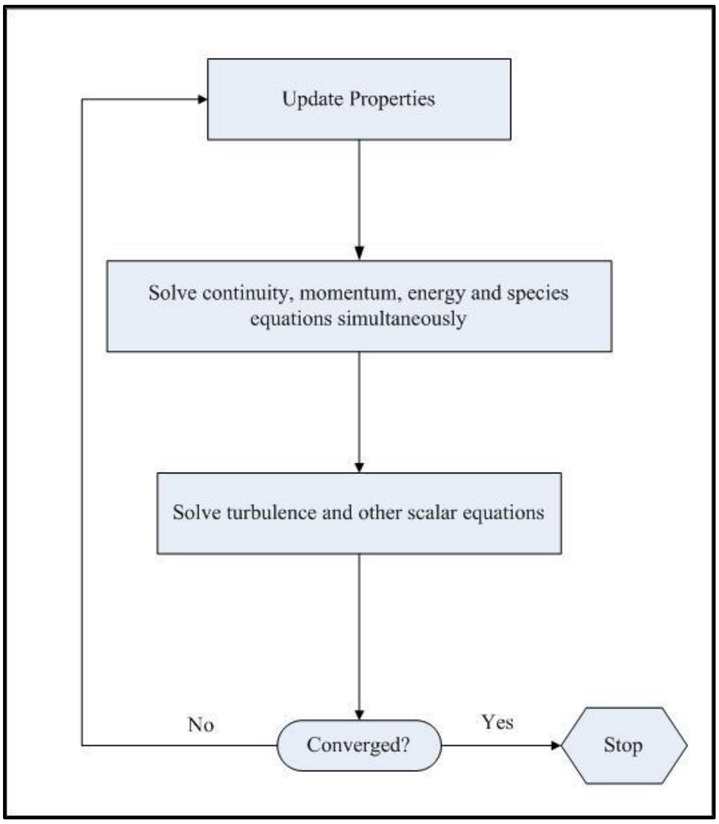

Figure 2-8: Density Based Solver Algorithm [23]

Discretization in FLUENT may be done by several ways. For spatial discretization, first or second order upwind scheme, central differencing scheme, power law scheme or higher order schemes are available. For temporal discretization, either first or second order schemes are available. Implicit or explicit types are also available.

As stated before, supersonic flow problem over a lateral jet controlled projectile contains turbulence in its nature. Turbulence may be defined as the irregular condition of flow in which the various quantities show a random variation with time and spatial coordinates [28]. The turbulence causes the transported flow quantities to fluctuate with respect to time in the field. Those fluctuations may be of very small scale and very high frequency. It is too computationally expensive for these kinds of flow aspects to be directly simulated.

In turbulent flow, eddying motion which is a large swirling motion exists. Energy containing large eddies are dissolved into smaller scale eddies and smaller scale eddies dissipate in the end. Kinetic energy contained in the large eddies is assumed equal to heat dissipation by small scale eddies.

There are mainly three types of approaches for numerical solution of Navier-Stokes equations. They are [29]:

- *Direct Numerical Simulation (DNS):* In this type of approach, from largest to smallest scales of eddies are resolved in a fluid flow. Eddies are the structures for transporting the turbulent quantities in a flow field. The time and length scales may be very small in a fluid flow. So the domain for numerical computations has to contain very fine meshes in order to simulate the flow with this technique. For example, when a flow with Reynolds number of 5000 is considered, approximately 45 billion grid points are required in the computational domain for a DNS run [30]. With the current computer technology, it is not possible to use DNS for high Reynolds number applications.
- *Reynolds Averaged Navier Stokes Approach (RANS):* Instead of resolving all scales of turbulence, in RANS approach whole range of eddies are not resolved but modeled by various turbulence models. Computational time is greatly reduced in RANS approach. In RANS, the solution variables are written as the sum of a mean and a fluctuating component. For example, for velocity vector in indicial form is written as;

$$u_i = \overline{u}_i + u_i^{'} \tag{2.14}$$

Where u_i is the i[th] component of velocity vector, $\bar{u}_i$ is the mean velocity component, u_i' is the fluctuating velocity component. After substituting the unknowns by the sum of a mean and a fluctuating component and rearranging the terms in momentum equation it becomes [23], [30]:

$$\begin{aligned} &\frac{\partial}{\partial t}(\rho u_i) + \frac{\partial}{\partial t}(\rho u_i u_j) = \\ &-\frac{\partial p}{\partial x_i} + \frac{\partial}{\partial x_j}\left[\mu\left(\frac{\partial u_i}{\partial x_j} + \frac{\partial u_j}{\partial x_i} - \frac{2}{3}\delta_{ij}\frac{\partial u_k}{\partial x_k}\right)\right] + \frac{\partial}{\partial x_j}(-\rho\bar{u}_i\bar{u}_j) \end{aligned} \tag{2.15}$$

Modification of momentum equation yields to new terms such as $-\rho\bar{u}_i\bar{u}_j$ This term is called "Reynolds Stress" term. In order for numerical solution to be completed, this term also must be modeled.

There are two approaches for modeling the Reynolds Stress term. First one is the "Boussinesq Approach", which relates the Reynolds Stress term to the mean velocity gradients.

$$-\rho\bar{u}_i\bar{u}_j = \mu_t\left(\frac{\partial u_i}{\partial x_j} + \frac{\partial u_j}{\partial x_i}\right) - \frac{2}{3}\left(\rho k + \mu_t\frac{\partial u_k}{\partial x_k}\right)\delta_{ij} \tag{2.16}$$

Where k is the turbulent kinetic energy and μ_t is the turbulent viscosity. These variables are additional unknowns to the primary unknowns in the governing equations. Turbulence models are introduced in this step for modeling of these unknowns. There are various turbulence models. In one equation turbulence models such as Spallart-Allmaras, one additional transport equation is solved. In two equation turbulence models such as k-ε turbulence model, turbulent viscosity is written as a function of turbulent kinetic energy k and turbulent dissipation rate ε and two additional transport equations are solved.

Alternative to Boussinesq Approach, Reynolds Stress Model is also used for modeling the Reynolds Stresses. In this model, additional transport equations are solved for the terms in the Reynolds Stress Tensor. Seven additional transport equations have to be solved in this method compared to maximum two in Boussinesq approach.

- *Large Eddy Simulation (LES):* In LES approach, larger eddies are resolved directly and smaller eddies are modeled. This method is the combination of DNS and RANS approaches. It requires less computer source than DNS but more than RANS. In today's computer technology, hardware demand is quite high for LES simulations. Figure 2-9 summarizes the approaches used for turbulence modeling.

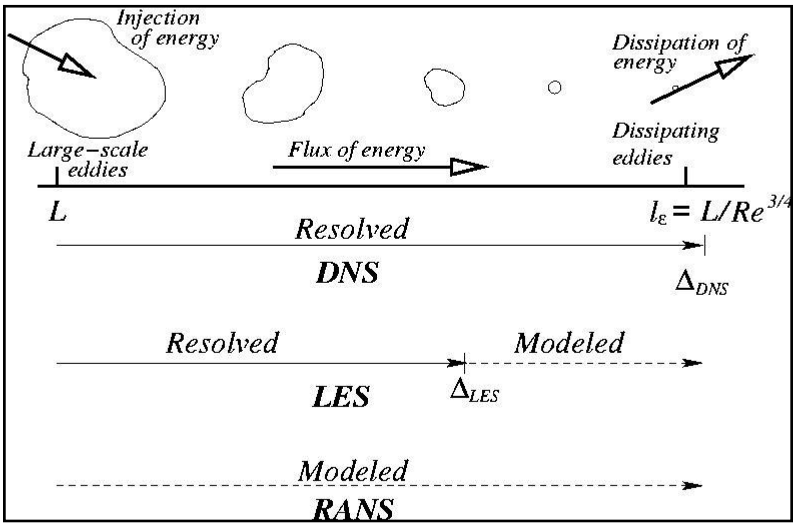

Figure 2-9: Turbulence Modeling Approaches

Besides turbulence models, different wall treatment options are available in FLUENT. There are mainly two approaches in dealing with wall bounded turbulent flows. First approach is the standard wall function approach and second one is the enhanced wall treatment approach. There are three zones in the near wall region. First one is the viscous sub layer, which is the zone in which flow is mostly laminar and viscosity is dominant. In fully turbulent zone, flow is fully turbulent and inertial effects are dominant. A transition region stands in between. In Figure 2-10, properties of the near wall region are shown [31].

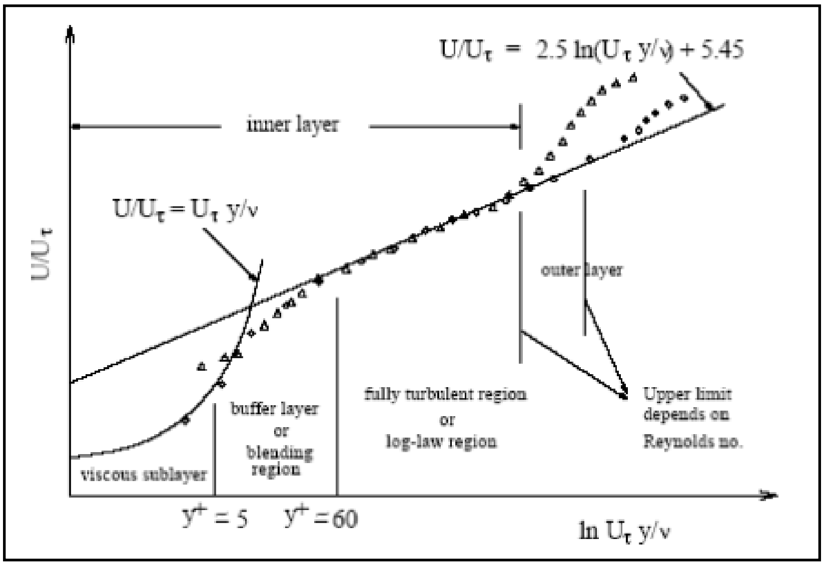

Figure 2-10: Flow Properties in Near Wall Zone [25]

Parameters in Figure 2-10 are defined in below equations. y^+ is a parameter in calculating the distance between the wall boundary condition surface and the first adjacent cell face, u_τ is the friction velocity, U is the free stream velocity and $\bar{C}_f$ is the skin friction coefficient estimated from flat plate.

$$y^+ = \frac{y u_\tau}{\nu} \tag{2.17}$$

$$u_\tau = \sqrt{\tau_w / \rho} = U\sqrt{\bar{c}_f / 2} \tag{2.18}$$

$$\bar{c}_f / 2 = 0.037 \mathrm{Re}_L^{-0.2} \tag{2.19}$$

For standard wall function approach, first cell should be located in turbulent zone and its y^+ value should be around 100. In enhanced wall treatment option mesh near the wall should be finer than in standard wall function option, y^+ should be below 5. In general, enhanced wall treatment option is recommended when there is wall driven turbulence in the flow [23].

General options for numerical solutions in FLUENT are given above. In the numerical runs to be used in the thesis, density based, steady solver will be used since it is highly recommended for high speed supersonic flows. In supersonic flow, conservation equations are highly coupled. Enhanced wall treatment type is selected to better capture the separation regions upstream of the jet exits, as recommended in literature [2]. One of two 2 equation turbulence models (RANS), k-ε and k-ω, will be selected after a turbulence model study one of the test cases. Analyses will be started with first order spatial discretization and after convergence is achieved, second order spatial discretization will be used. For convergence, axial, normal forces and pitching moment convergence histories for missile models will be considered. When the percent difference between last and last 100^{th} iteration is less than %1 and percent difference between arithmetic averages of last 100 and previous last 100 (last 100-200) are less than %1, convergence will be achieved and simulations will be stopped.

CHAPTER 3

VALIDATION STUDIES

Two test models are selected for the purpose of validating the numerical tools and techniques. The models are missile like geometries, which have side jets and which are tested in wind tunnels in supersonic free stream conditions. Details of the models are given in sub sections.

3.1 Test Model 1

Test Model-1 (TM-1) is a generic projectile shape consisting of several configurations [14]. The model consists of a tangent ogive nose of 2 calibers and a cylindrical after body of 3.8 calibers. There is a circular, sonic nozzle placed 2.5 calibers from the nose tip on the upper part of the model. Diameter of the model is 50 mm. The nozzle has a diameter of 5mm. The control surface of this model has a leading edge sweep angle of 45º, 0.5 diameter semi span and 1.4 diameter root chord. Two configurations are considered in this study and shown in Figure 3-1.

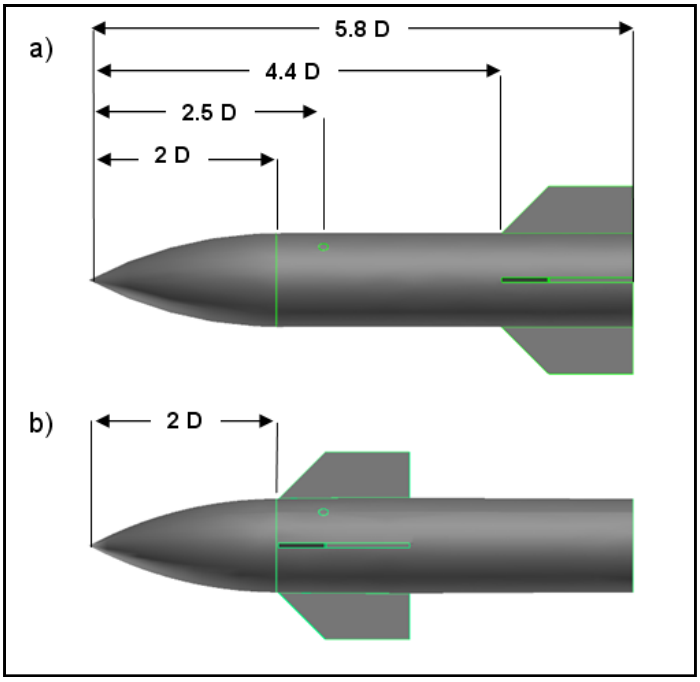

Figure 3-1: Test Model 1 Dimensions a) Body Tail (BT) b) Body Canard (BC)

The models were tested in a wind tunnel in Israel Aircraft Industries at free stream Mach numbers of 2, 3.3, 4.5 and 8. The model is placed in the sting balance in "*X*" configuration; i.e. the jet nozzle is in vertical orientation. The injected gas used in the experiments was nitrogen, but it was assumed air in the numerical calculations. Experiments were carried out for several angles of attack between -15° and 15°. In this part, Mach number of 2 experiments is simulated by CFD. Ambient and jet conditions in the experiments are given in Table 3-1.

Table 3-1: TM-1, Experimental Conditions

Ambient conditions		Jet Conditions BC		Jet Conditions BT	
M	2	M	1	M	1
P [Pa]	24721,2	P [Pa]	1821187	P [Pa]	1456949
P_0 [Pa]	191295	P_0 [Pa]	3447379	P_0 [Pa]	2757903
T [K]	170	T [K]	215	T [K]	235,26
T_0 [K]	306	T_0 [K]	258	T_0 [K]	282
S_{ref} [m^2]	0,001963	$\dot{m}$[kg/s]	0,17	$\dot{m}$[kg/s]	0,13
L_{ref} [m]	0,05	A_{jet} [m^2]	0,000019	A_{jet} [m^2]	0,000019
V	522,8	V_{jet} [m/s]	294,0	V_{jet} [m/s]	307,5
ρ[kg/m^3]	0,507	F_{jet} [N]	84,10739	F_{jet} [N]	67,18821

In the experiments for ambient and jet conditions; Mach numbers, stagnation pressures and temperatures are given. For jet conditions, mass flow rates are also specified. From given parameters, necessary input parameters are calculated. Sample calculations and necessary input conditions in FLUENT are given in Appendix for Test Model 1.

For CFD runs, missile like geometries are located in large enough cylindrical domains. For the faces of cylindrical domain, *pressure far field* boundary condition is selected. Ambient Mach number, static pressure and temperature are inputs for this boundary condition. For jet exits, *mass flow inlet* type is selected. For this boundary condition, mass flow rate, static pressure and total temperature are inputs. For the model parts, *wall* boundary condition with no slip option is selected.

In following figures; domain and boundary conditions, surface elements, boundary layer cells and volume cells samples can be seen.

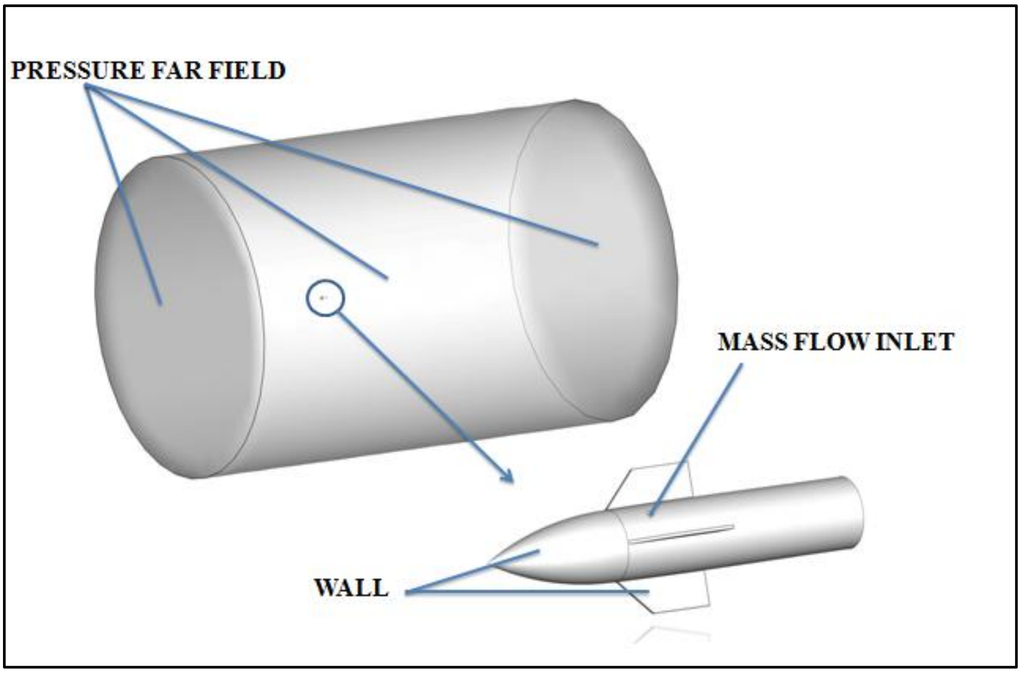

Figure 3-2: Flow Domain and Boundary Conditions

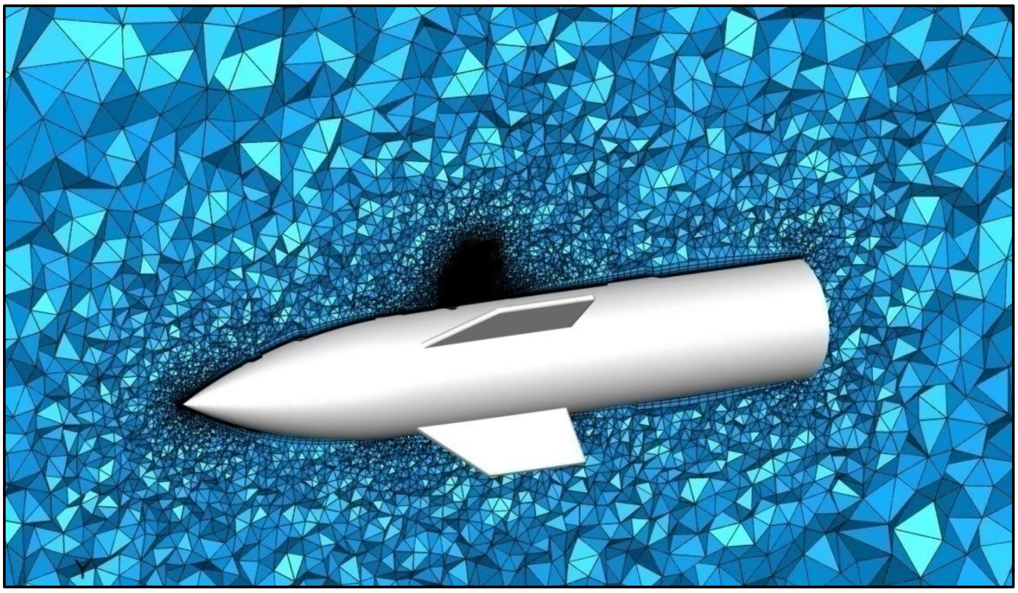

Figure 3-3: TM-1, Volume Cells

Volume grid and surface grid around the jet exit has been made denser by using the sizing functions. Total number of cells is slightly higher than 3 million.

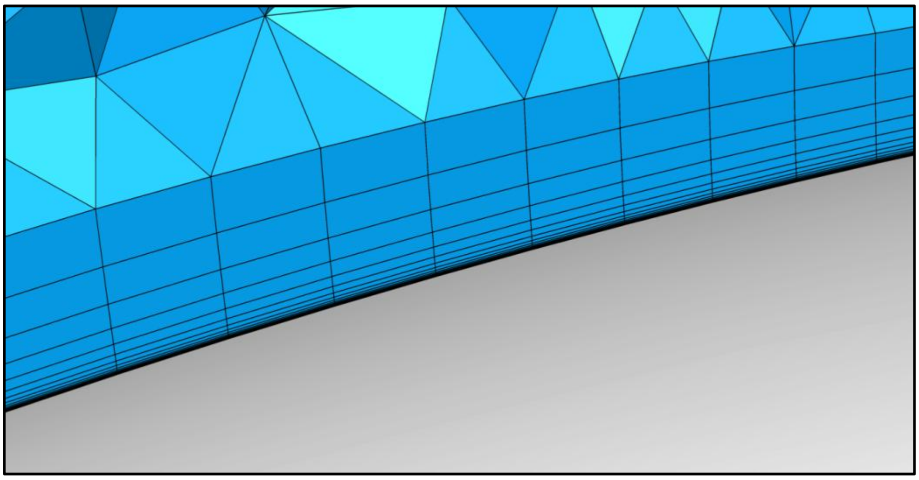

Figure 3-4: TM-1, Boundary Layer Cells

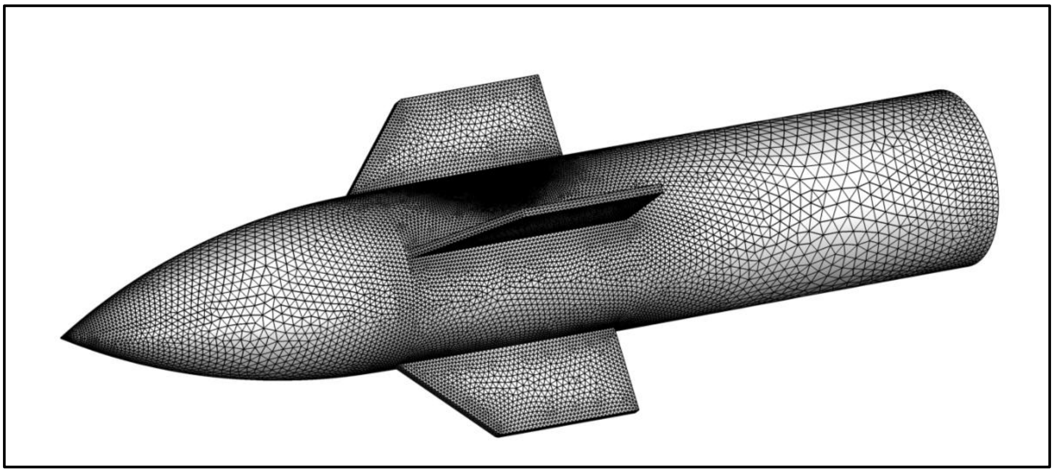

Figure 3-5: TM-1, Surface Grid

As the results of experiments of TM-1, two parameters are reported. They are force amplification factor K and center of pressure shift X_{CPi}. They are defined as:

$$K = \frac{C_{N-jet,on} - C_{N-jet,off}}{C_{N-jet}} \tag{3.1}$$

$$X_{CPi} = \frac{C_{M-jet,on} - C_{M-jet,off}}{C_{N-jet,on} - C_{N-jet,off}} \tag{3.2}$$

Force amplification factor K is a measure of how the interaction of jet and the free stream affect the normal force. If K is greater than 1, normal force is amplified by the interaction, i.e. difference in normal force between jet-on normal force and jet-off normal force is greater than jet alone normal force. If K is less than 1, normal force is de-amplified by interaction. X_{CPi} is the measure of the distance where the combination of interaction forces act with respect to the moment reference center. It is a characteristic jet interaction moment length scale. These parameters from experiments will be compared with the ones obtained from CFD, to see how well the problem is solved with numerical tools.

For CFD runs of TM-1, fourteen runs are made for seven different angles of attack for each configuration. Angles of attack are from -12º to 12º with 4º increments.

Calculation of parameters K and X_{CPi} requires force and moment coefficient values for both jet-on and jet-off conditions. So for both configurations, jet-off CFD runs are also carried out for entire angle of attack range.

3.1.1 Turbulence Model Study

For TM-1 with BC configuration, first a turbulence model study is conducted. Two turbulence models are chosen for comparison with experiments. They are k-ε and k-ω turbulence models. As discussed in second chapter, they are two equation turbulence models which use RANS approach. They are two most commonly used models in Aerodynamics division of ROKETSAN for CFD analysis.

In Figure 3-6 and Figure 3-7, experimental results for K and X_{CPi} are compared with results of CFD runs with two different turbulence models.

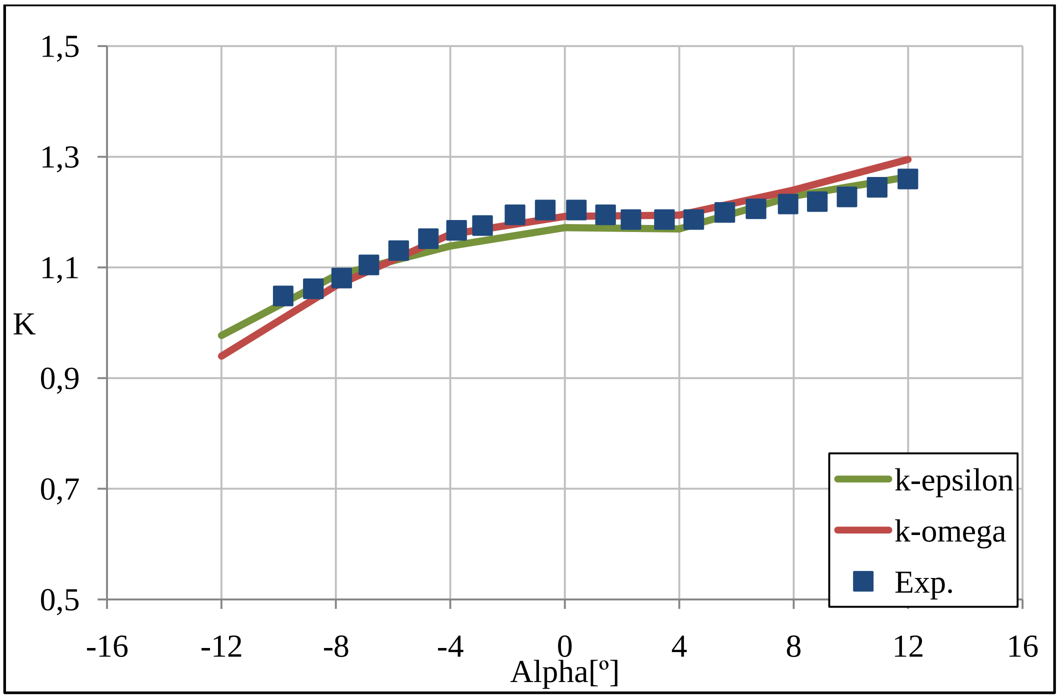

Figure 3-6: TM-1 BC, Turbulence Model Comparison for *K*, M= 2

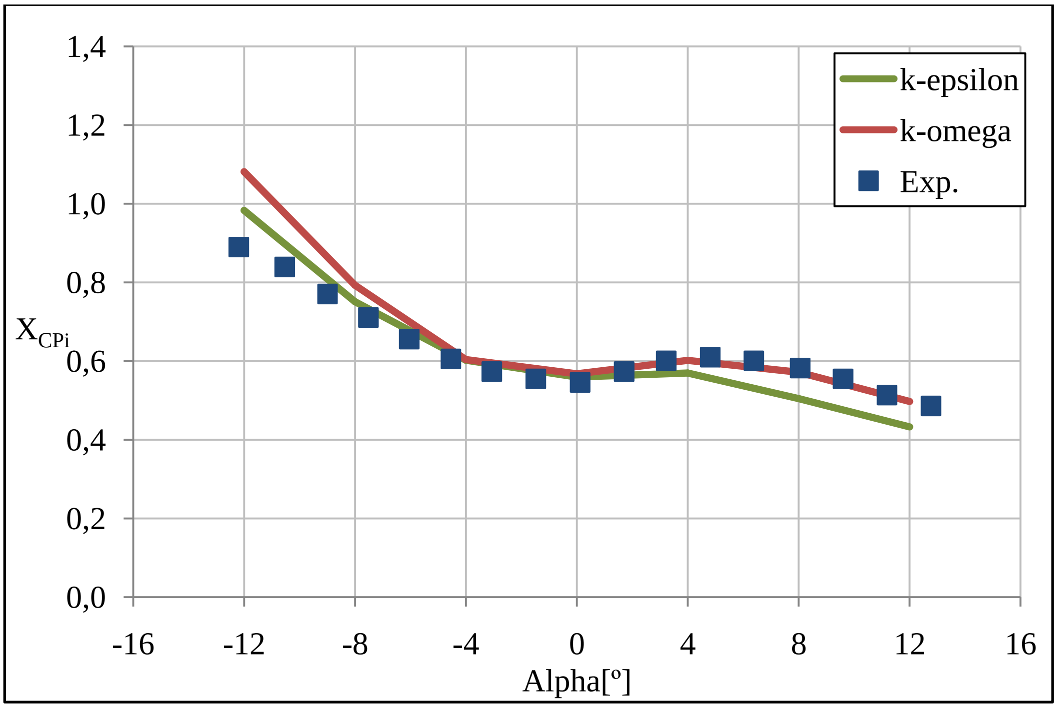

Figure 3-7: TM-1 BC, Turbulence Model Comparison for X_{CPi}, M= 2

If Figure 3-6 and 3-7 are examined, for both models CFD results are in good agreement with experimental results. For K values, maximum error is less than %8 in entire angle of attack range. For X_{CPi} values k-ω turbulence model has less error in positive angles of attack than k-ε model and more error in negative angles of attack. Maximum error in X_{CPi} is less than %20 percent for k- ω and less than %11 for k-ε. But it takes 3500 iterations for k- ω to converge whereas it takes 2500 iterations for k-ε model. 3500 iterations take about 10 hours in two nodes of a cluster computer, which has four processors per node and four gigabytes of ram per processor. 2500 iterations take about 6 hours.

For better understanding of the differences between CFD runs for two different turbulence models, following figures are presented. In following figures, surface pressure coefficient values for two different turbulence models are shown for both jet-on and jet off conditions, for zero angle of attack. Surface pressure coefficient C_P is defined as:

$$C_P = \frac{P - P_\infty}{0.5 q S_{REF}} \tag{3.3}$$

Where P is the static pressure at an arbitrary location, P_∞ is the free stream static pressure, q is the free stream dynamic pressure and S_{REF} is the reference area, which is the cross sectional area.

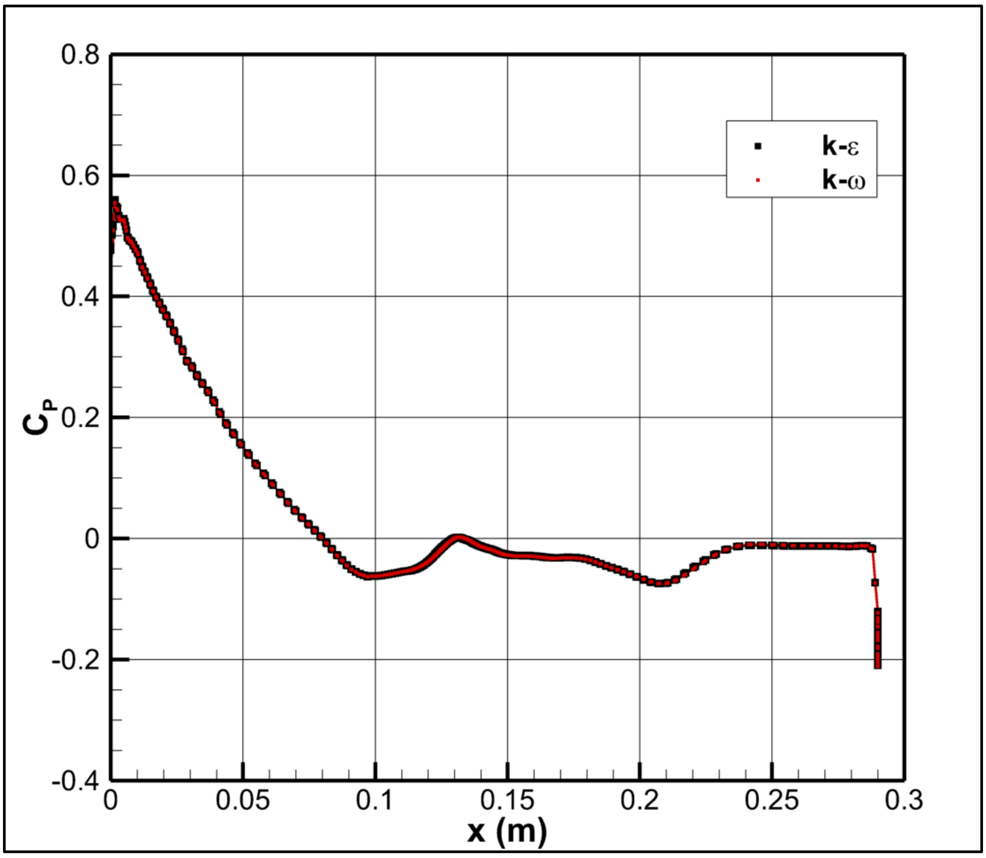

Figure 3-8: TM-1 BC, C_P comparison for turbulence models, jet-off, α= 0°

If Figure 3-8 is examined, C_P values calculated from two different turbulence model simulations are very close to each other. It should be noted that the x axis of the curve corresponds to intersection of x-z plane from Figure 1-1 with the upper part of the missile body. Surface pressure distribution is typical for a supersonic missile like body. Pressure increases at the nose due to bow shock and slowly decreases due to convex geometry of the nose. Pressure is slightly increased round the leading edges of the lifting surfaces due to compression and decreases at the trailing edges due to expansion. Towards the end of the body, pressure is slowly increased to free stream value and sharply decreases at the base due to intense flow separation.

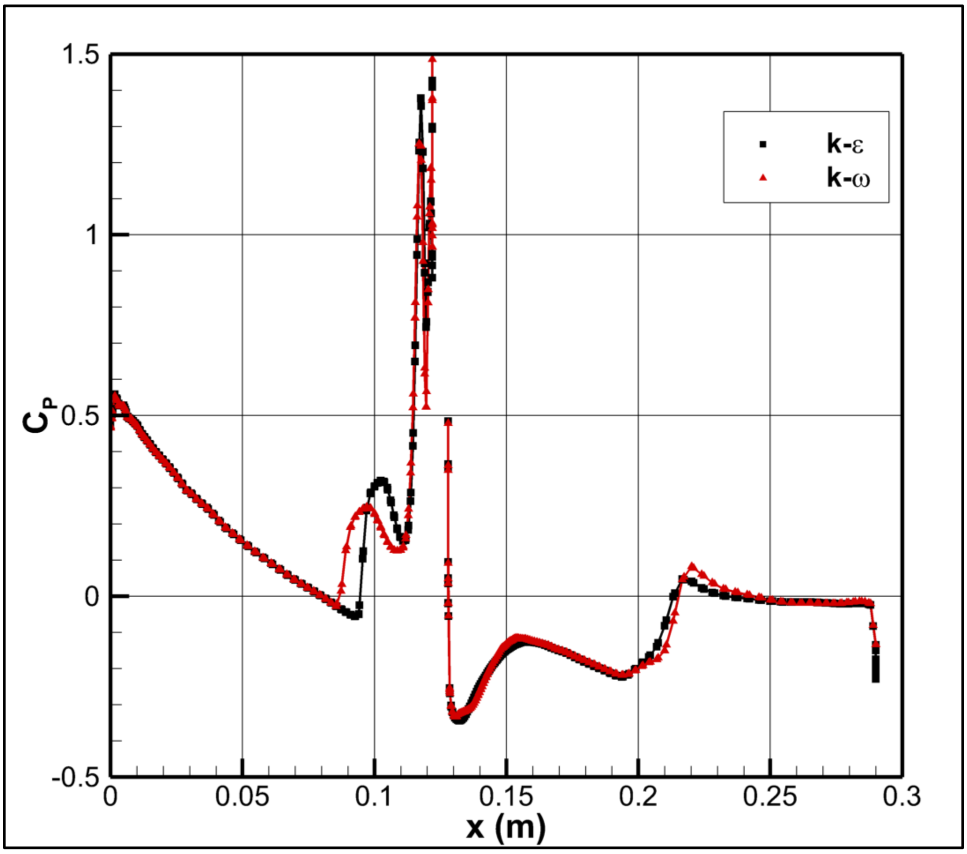

Figure 3-9: TM-1 BC, C_P comparison for turbulence models, jet-on, α= 0°

Figure 3-9 is the comparison of surface pressure values for both turbulence models when the jet is active. Two curves are similar to each other except the jet upstream zone. For k-ε model, first peak of the pressure curve is located closer to the jet exit and pressure value is higher than k-ω model. This difference can also be seen in following figures, which show the surface pressure distributions on the models for two different turbulence models. Upstream influence zone is larger in k-ω model but maximum pressure for this zone is higher in k-ε model. In following figures, legend is set to 0-50000 Pa.

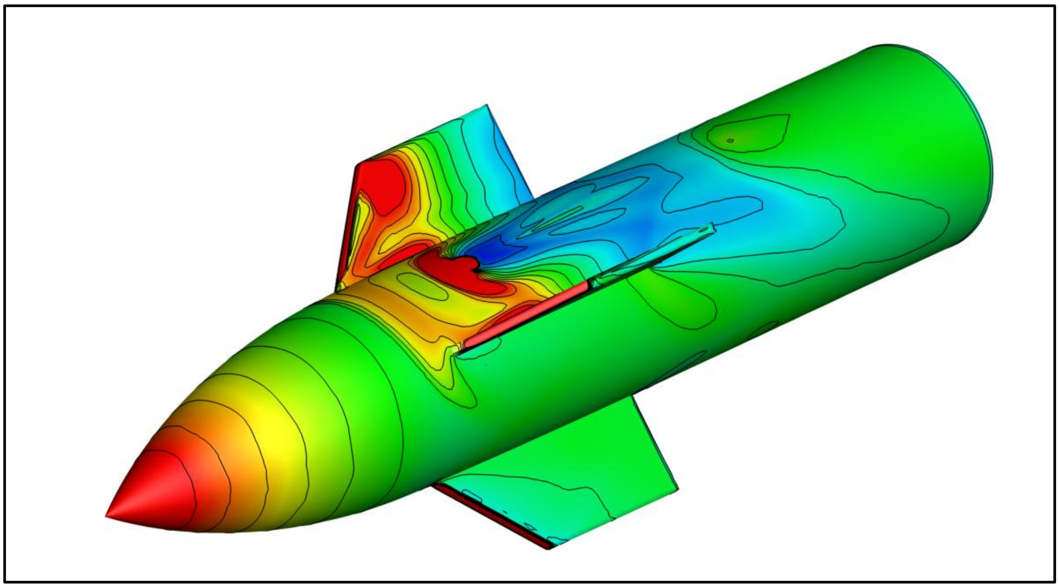

Figure 3-10: TM-1 BC, Surface pressure distribution on model, k-ε turbulence model

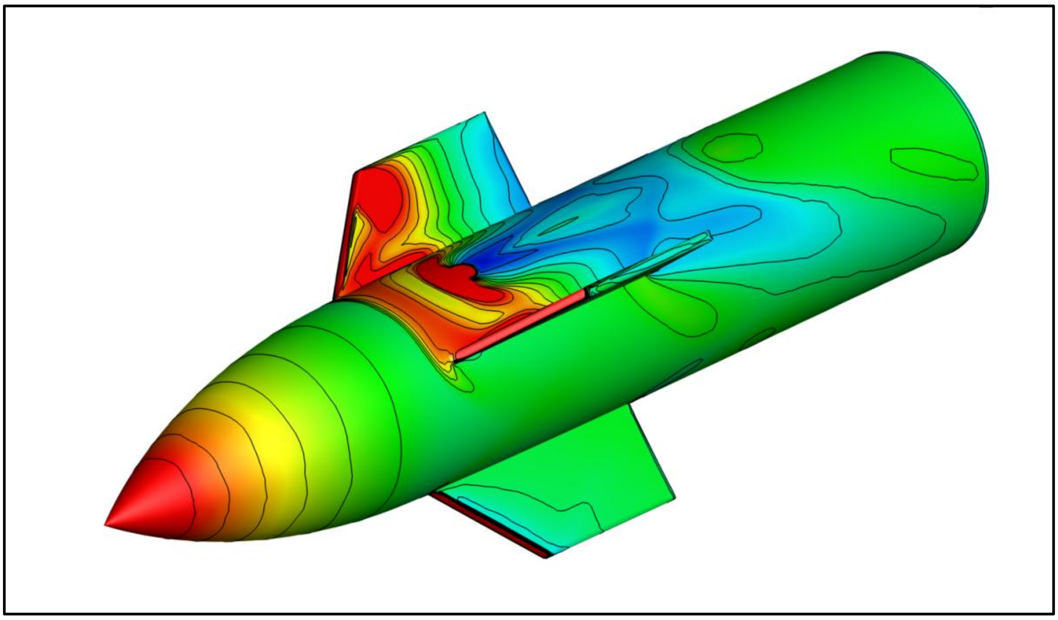

Figure 3-11: TM-1 BC, Surface pressure distribution on model , k-ω turbulence model

It should be noted that techniques introduced in Chapter 2 are used in k-ε model. For k-ω model, Shear Stress Transport option is selected. Considering the errors and convergence time, k-ε model is selected to be used in the rest of the study. Calculation of K and X_{CPi} values require both jet-on and jet-off results so these values contain errors from two separate simulations. In Appendix, tables for analysis results for TM-1 and sample calculations are given.

3.1.2 Results

For two configurations of TM-1, comparison of K and X_{CPi} values between experimental results and CFD results are shown in following figures.

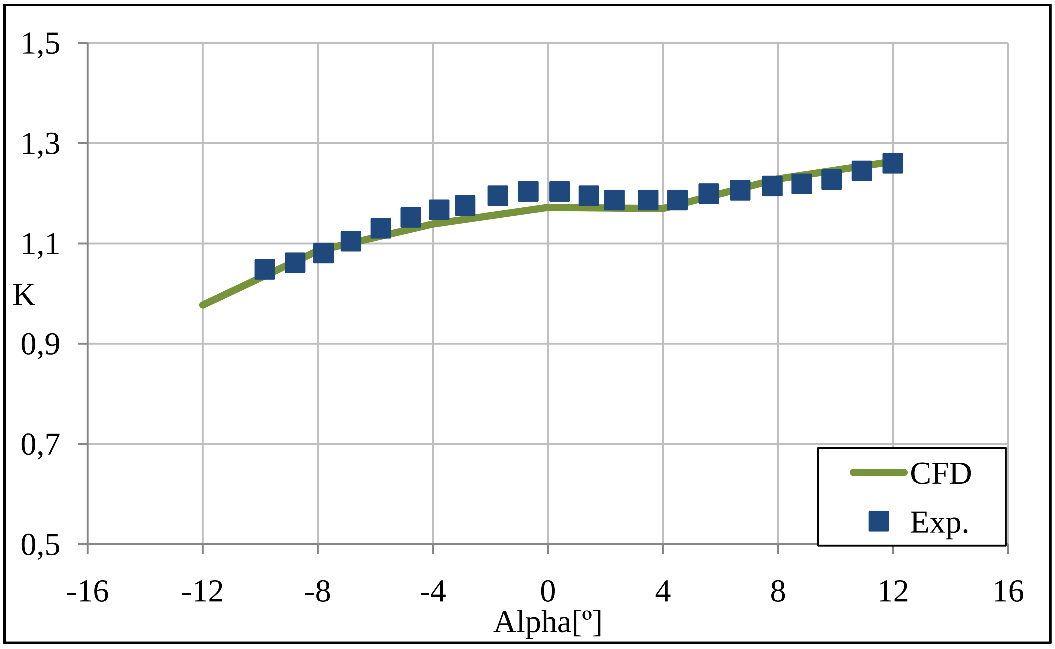

Figure 3-12: TM-1 BC, M= 2, Comparison of *K* Values

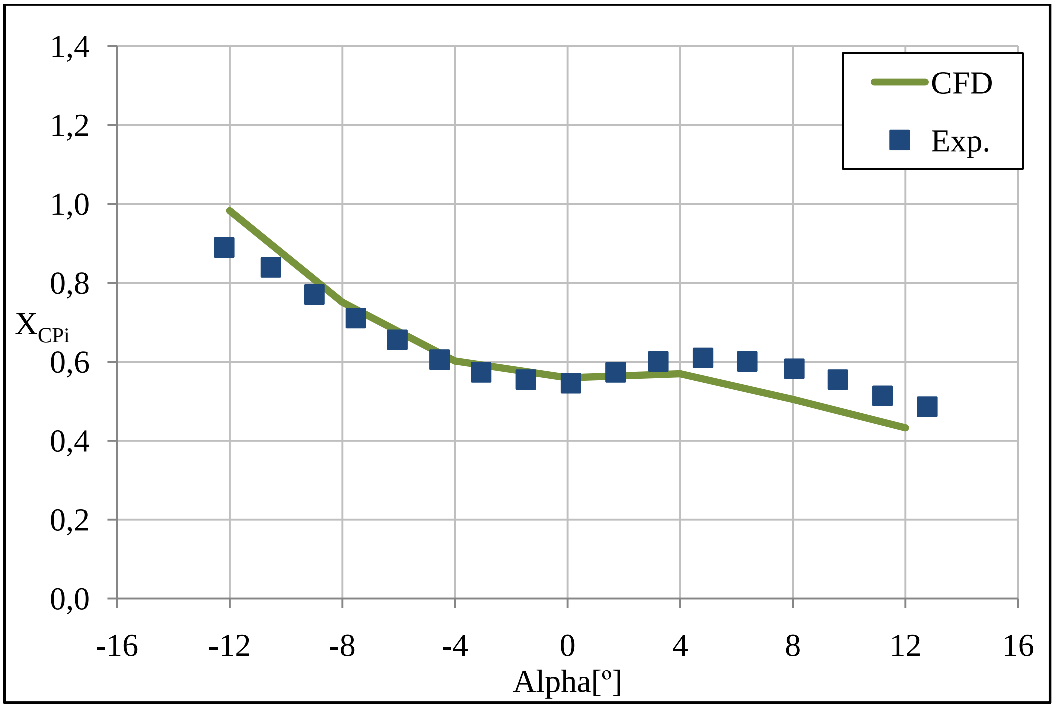

Figure 3-13: TM-1 BC, M= 2, Comparison of X_{CPi} Values

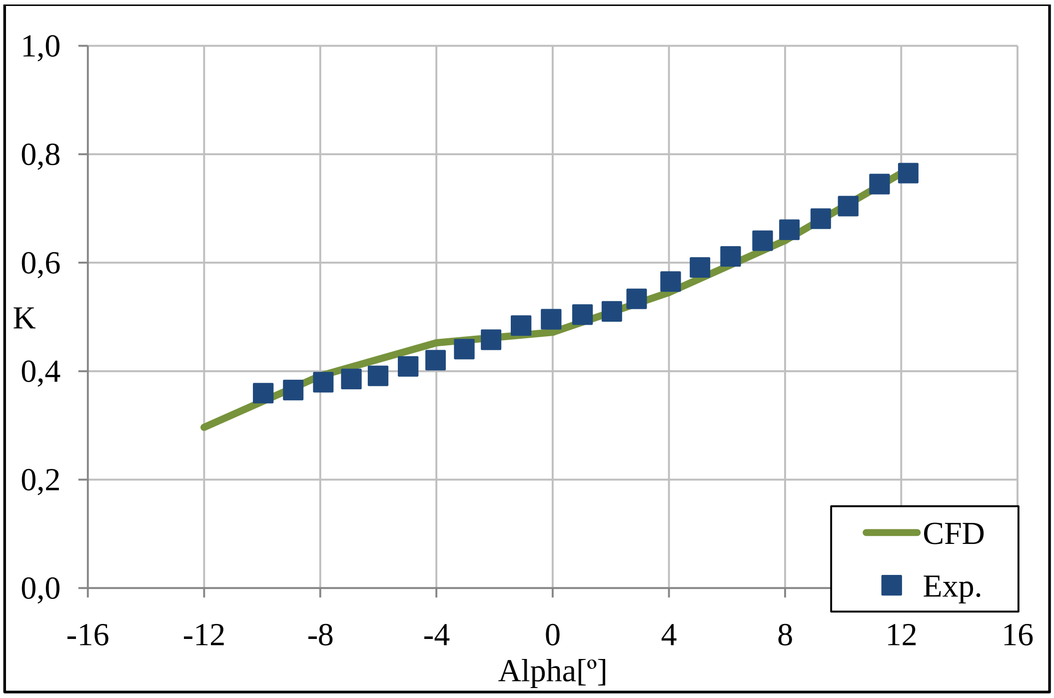

Figure 3-14: TM-1 BT, M= 2, Comparison of *K* Values

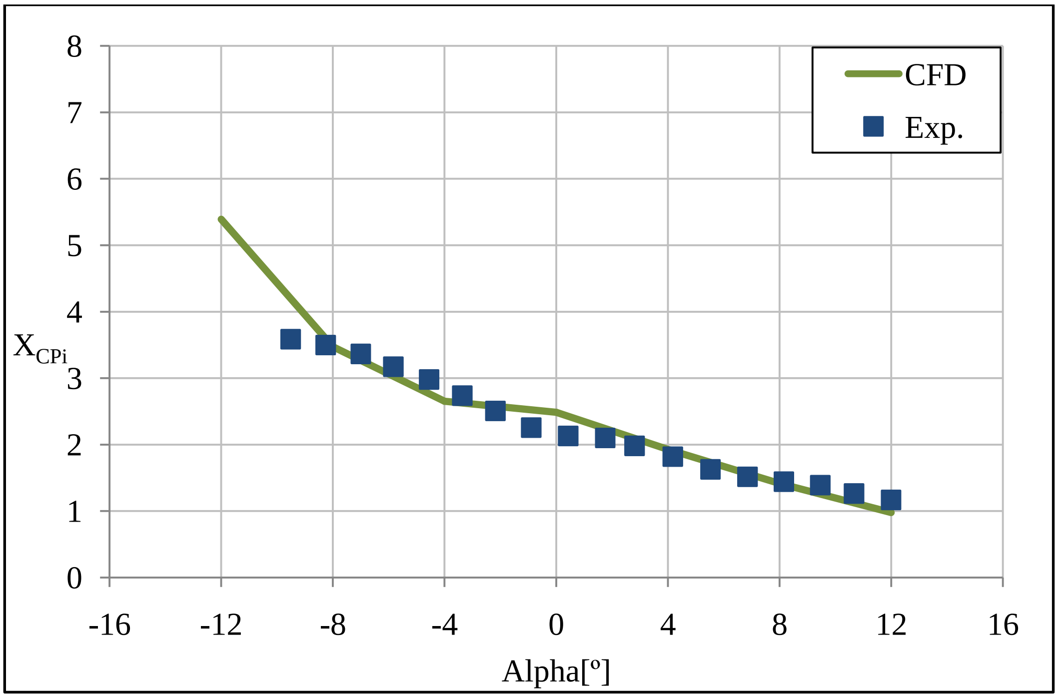

Figure 3-15: TM-1 BT, M= 2, Comparison of X_{CPi} Values

If Figures 3-12 to 3-15 are examined, experimental results agree well with CFD results. Maximum error is %8 for K values and %11 for X_{CPi} values. In K curves, it is obvious that force is amplified more in BC configuration. K is greater than 1 in entire angle of attack range whereas in BT configuration, it is less than 1. It means that for the former configuration jet-alone normal force is amplified whereas in the latter configuration it is de-amplified. In Figures 3-16 and 3-17, static pressure distribution around the model and pitch plane is shown. If these figures are examined carefully, low pressure region caused by the jet is larger in the BT configuration than in BC configuration. This lower pressure indicates that total normal force acting on the model decreases. Also in BC configuration, lifting surfaces are closer to jet exit. Presence of high pressure fluid increases surface pressure on the upper surfaces of canards and this physical interaction can be seen in Figure 3-10 and Figure 3-11. Increasing the pressure on the upper surfaces of the lifting surfaces make more contribution to normal force created by the upward ejecting jet.

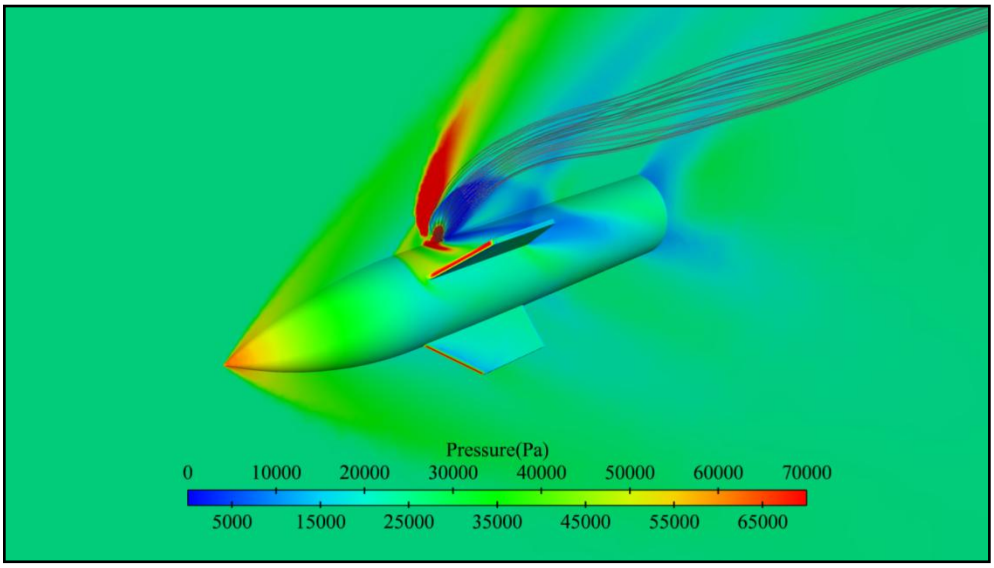

Figure 3-16: TM-1 BC, Static Pressure Distribution and Jet Exit Streamlines, M=2, α= 0º

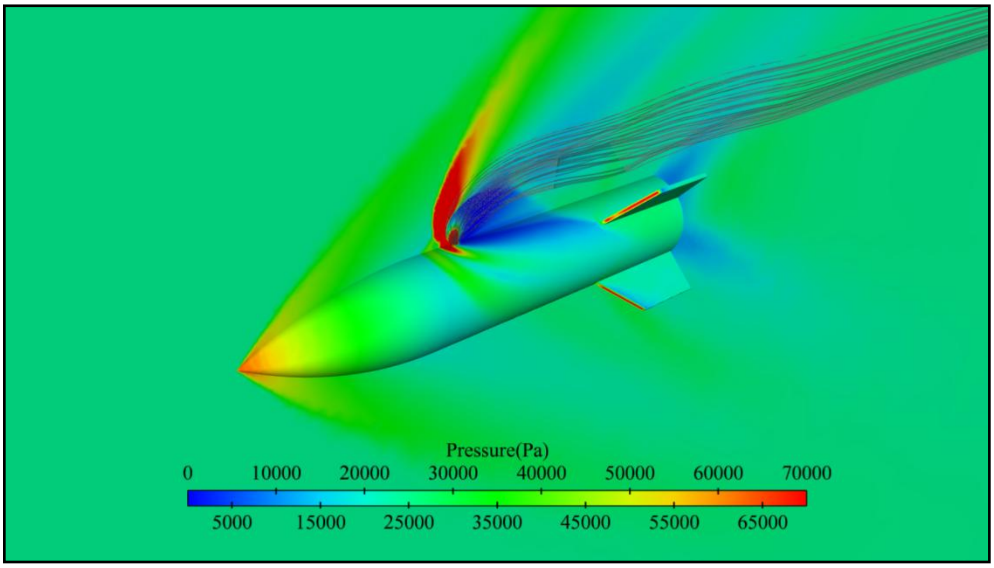

Figure 3-17: TM-1 BT, Static Pressure Distribution and Jet Exit Streamlines, M=2, α= 0

For BT configuration, force amplification decreases with negative angles of attack. At positive angles of attack, jet wake is directed away from the tail fins where in negative angles of attack, jet wake is directed onto tails, as reported in literature [32]. In negative angles of attack and in the absence of the jet, pressure in the upper surfaces of lifting surfaces is increased and negative normal force is created. When the jet wake is directed onto the tails in presence of jet, increase of the surface pressure on the upper surfaces of tails is denied to some extent. These results in decrease in jet-on normal force thus decrease in *K* value. In Figure 3-18 and Figure 3-19, surface pressure distributions on TM-1 BT for both jet-on and jet –off cases are shown at α= -12°. It can be seen that tail upper surface pressure is affected by the presence of the jet. Tail upper surface pressure values are higher in jet-off case.

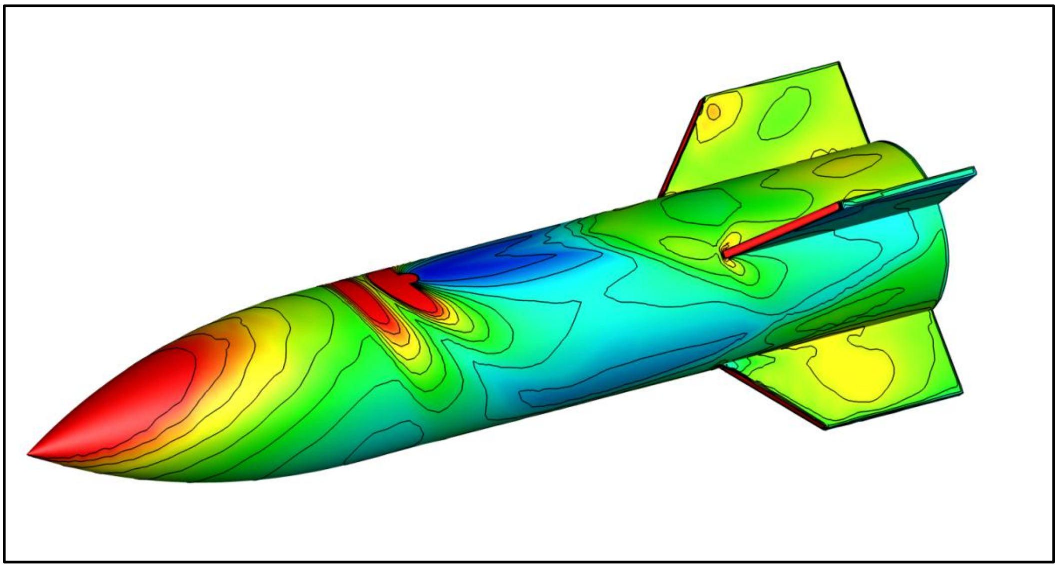

Figure 3-18: TM-1 BT, Surface Pressure Distribution, jet-on, α= -12°

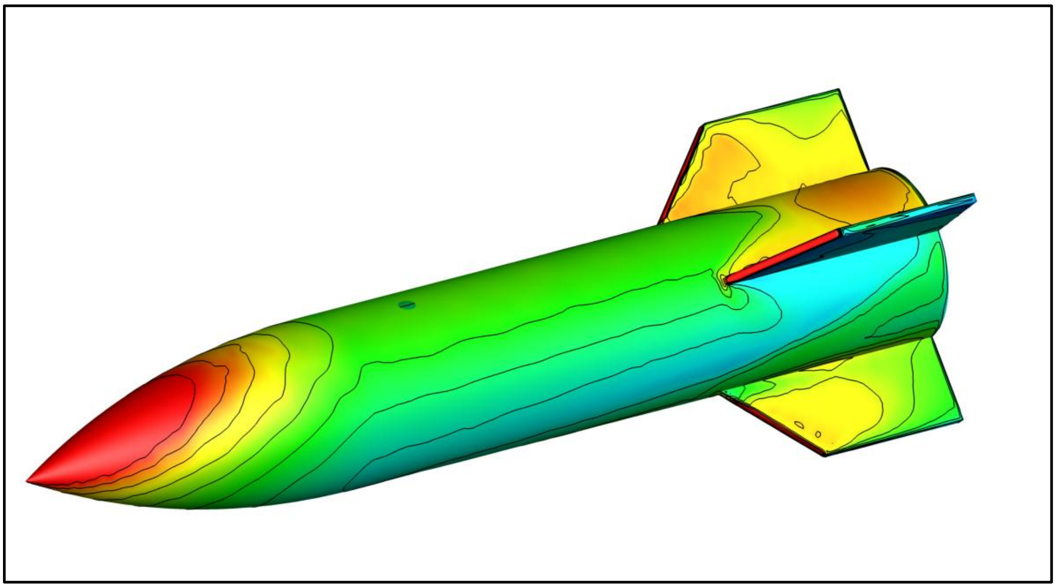

Figure 3-19: TM-1 BT, Surface Pressure Distribution, jet-off, α= -12°

As stated above, X_{CPi} is the measure of where interaction forces act with respect to moment reference center. In TM-1, moment reference center is the jet exit. In BC configuration, most contribution to jet interaction force comes from the canards, which are close to jet exit. Thus X_{CPi} values are lower than BT configuration; i.e interaction center is closer to moment reference center. In BT configuration, jet effects are spread to whole body of the model. Even tails are affected by the presence of the jet. Tails are located further away from the jet exit than canards so

X_{CPi} values are greater than tails. For both configurations, interaction moment center is located closer to jet exit at positive angles of attack, i.e. X_{CPi} values are lower. For positive angles of attack, jet is directed away from the body of the test model so that surface pressures are affected in smaller regions, in which case application point of the interaction force is closer to moment reference center.

As stated before, no jet condition CFD simulations are made for calculating K and X_{CPi} values. In Figure 3-20 and Figure 3-21, normal force and pitching moment coefficients for both configurations and for both jet-on and off cases are compared. It is obvious that normal force curves shift downwards when jet is active. Since force amplification is higher in BC, normal force values are reduced more in BC configuration, noting that jet alone normal force has a negative value since jet ejects upwards. In moment curves, for both configurations, pitch-down moment is added to the model when the jet is active. Jet exit location is the moment reference center; upstream high pressure zone and low pressure downstream zone create a pitch-down moment couple for both configurations..

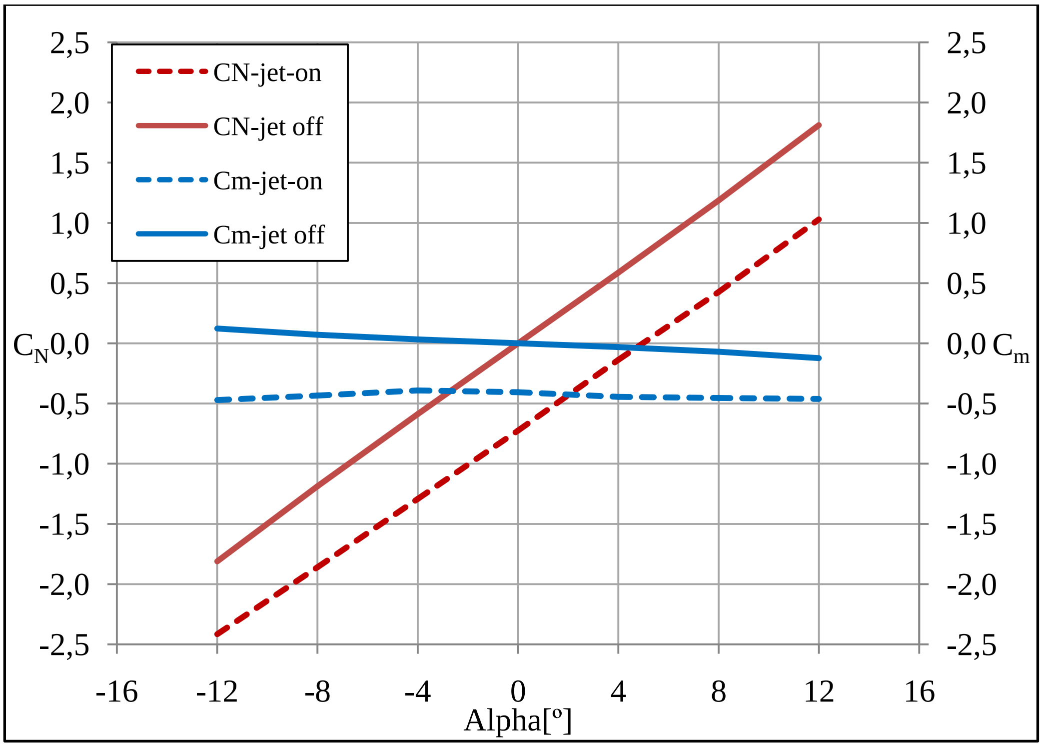

Figure 3-20: TM-1 BC, Jet-On and Off Force and Moment Comparison

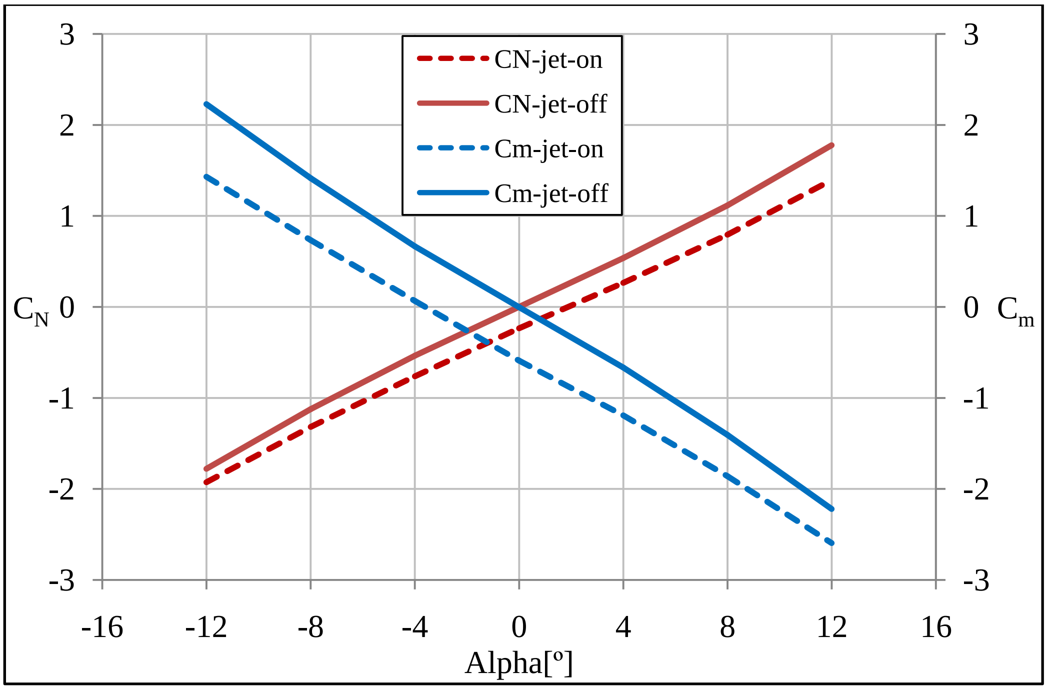

Figure 3-21: TM-1 BT, Jet-On and Off Force and Moment Comparison

3.2 Test Model 2

Test model 2 (TM-2) is a generic supersonic missile shape which has a conical nose, a cylindrical mid section and a flare aft body [7]. Model has 9 calibers length and 0.1 D sonic jet exit is located at 4.3 calibers downstream of the nose tip, shown in Figure 3-22. Diameter of the model is 40 mm.

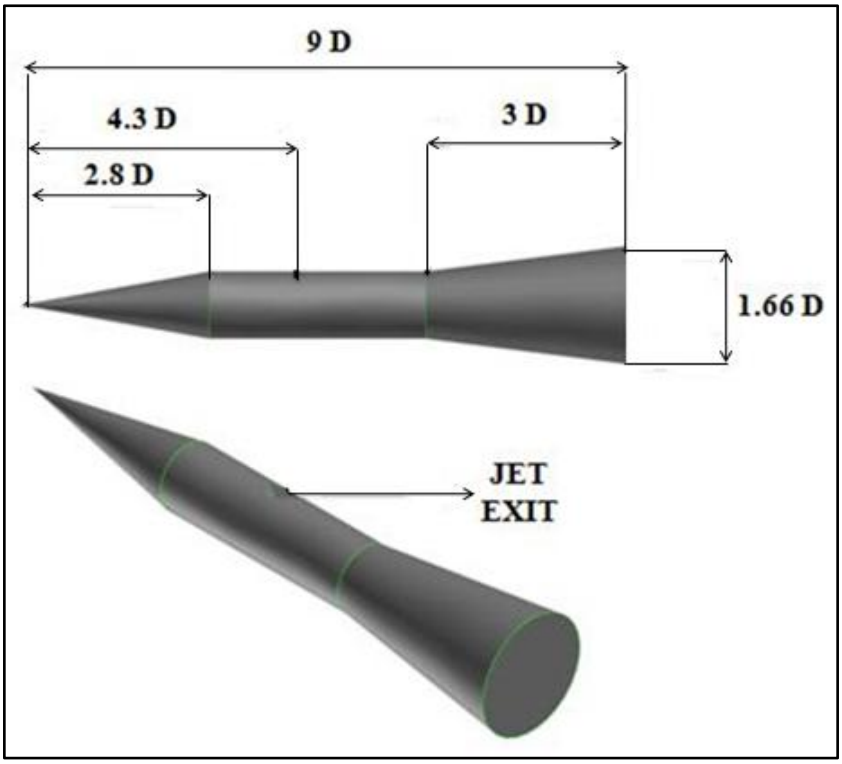

Figure 3-22: TM-2 Model Dimensions and Isometric View

For TM-2, pressure coefficient distribution for 180º, 150º and 120º roll angles (φ) in longitudinal direction are reported. Roll angle is measured from the base and clockwise, as 0° being the bottom point in *z* direction of the base. Ambient and jet conditions are given in Table 3-2. Jet temperature is not explicitly stated so that it is assumed to be equal to ambient temperature. Also the injected fluid is assumed air. The surface pressure is defined in TM-1 sub-chapter.

Table 3-2: TM-2 Ambient and Jet Conditions

Ambient conditions	
M	2.8
T[K	108.96
P[Pa]	20793.2
Jet conditions	
M	1
P_{jet}/P	100

Computational domain for TM-2 is done in similar fashion to TM-1. But total number of cells for TM-2 is slightly higher than 6 million mixed cells. A grid was created with size similar to TM-1, no results were obtained due to convergence problems. So a finer grid is made and convergence is achieved. Techniques used in the solution are the same as in TM-1 solutions.

3.2.1 Results

In following figures, experimental results and CFD results are shown for 180º, 150º and 120º roll angles. *"jet-l."* line corresponds to jet location.

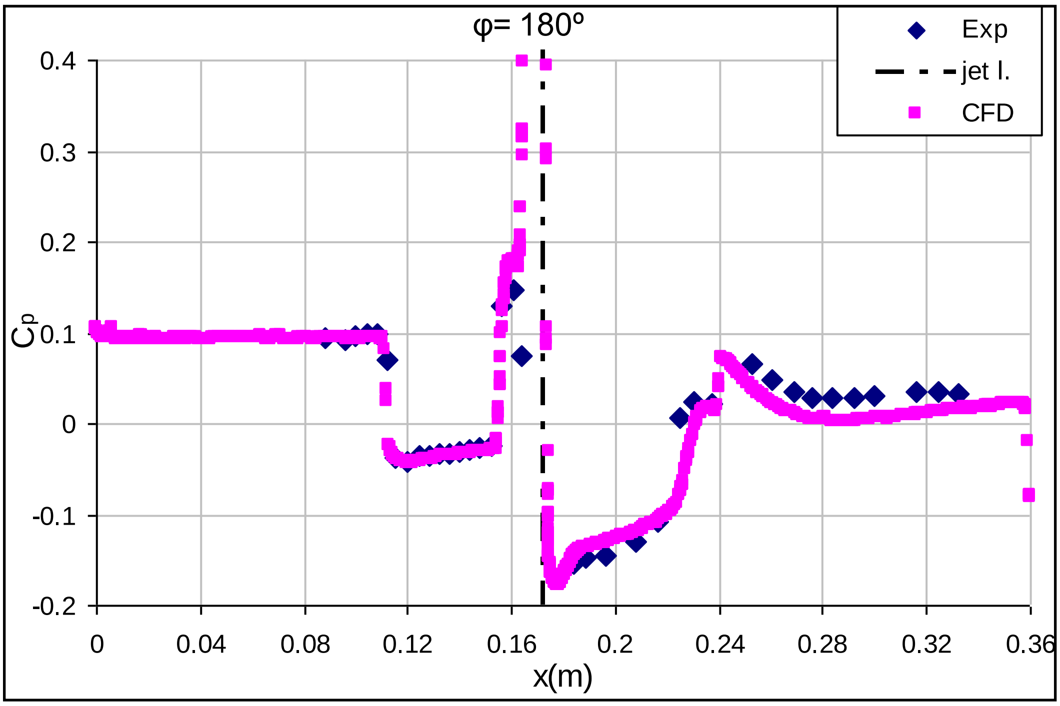

Figure 3-23: TM-2 Results for 180º Roll Angle

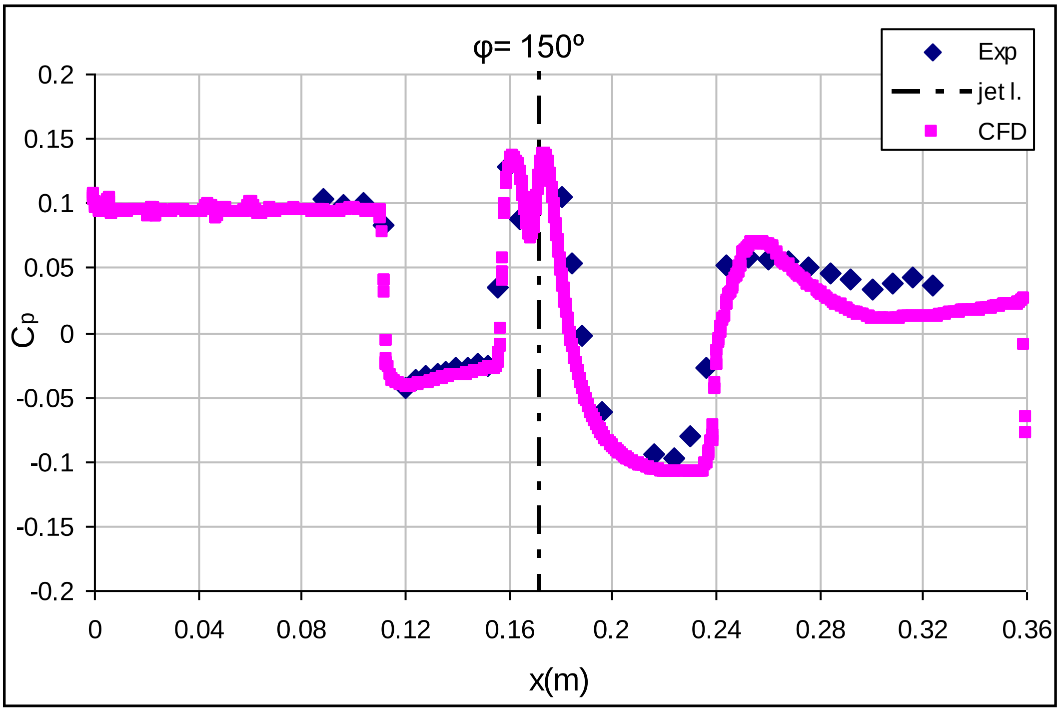

Figure 3-24: TM-2 Results for 150º Roll Angle

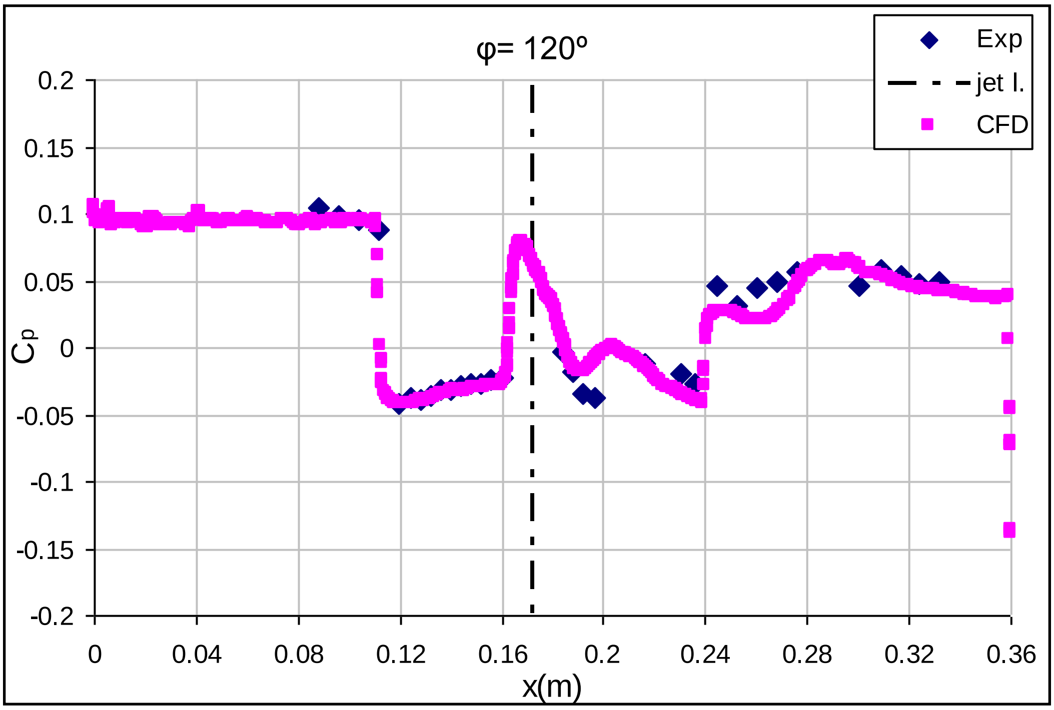

Figure 3-25: TM-2 Results for 120º Roll Angle

If above figures are examined, CFD results are in good agreement with experimental data, as in TM-1. Some discrepancies exist in the flare part and the separation part just upstream of the jet exit, but in overall the prediction capabilities of CFD are found adequate for this case. The jet effects diminish as the roll angle is increased further from 120º so further angle surface pressures are not compared. Errors for C_p values are large for 120º at about x= 0.2 m, but maximum error is %10 for surface static pressure values if calculated from C_p values. In Figure 3-26 and Figure 3-27, surface static pressure and Mach number distributions around TM-2 are shown. If Figure 3-26 is examined, flow structure is similar to TM-1. Nose bow shock and jet bow shock form a mixing region and downstream of the jet there is a low pressure region due to jet being like an obstacle to the flow.

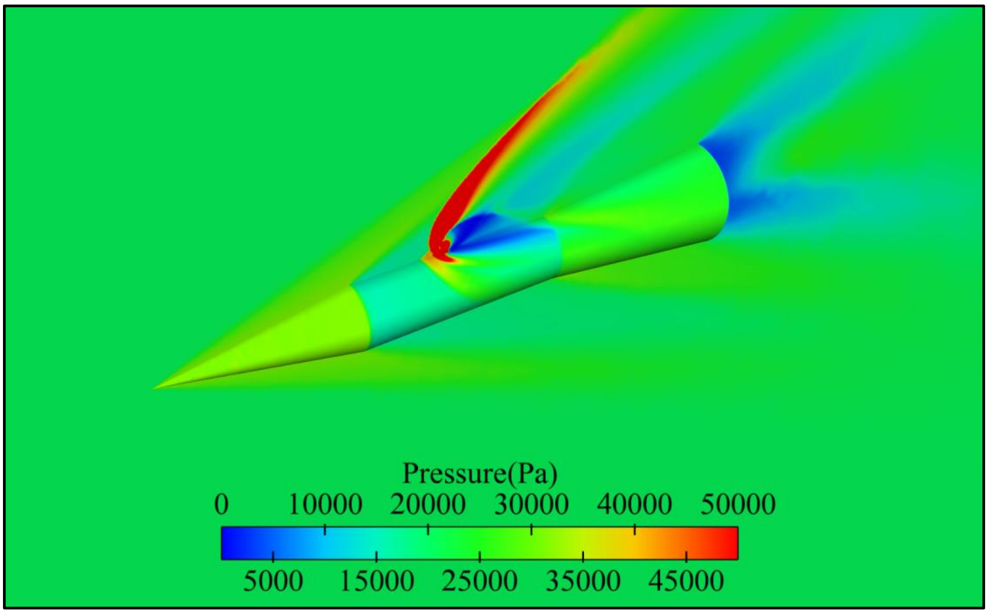

Figure 3-26: TM-2, Static Pressure Distribution around the Model

In Figure 3-28, close up picture of jet exit is shown. It is clear from this figure that most of the prominent features of the complicated flow are captured by the CFD analysis .In this figure, *1* is the nose bow shock. *2* is the jet bow shock and *3* is the upstream separation zone. *4* is the jet expansion region caused by high pressure jet exiting to free stream. Lastly *5* is the recompression shock to orient the flow parallel to the model.

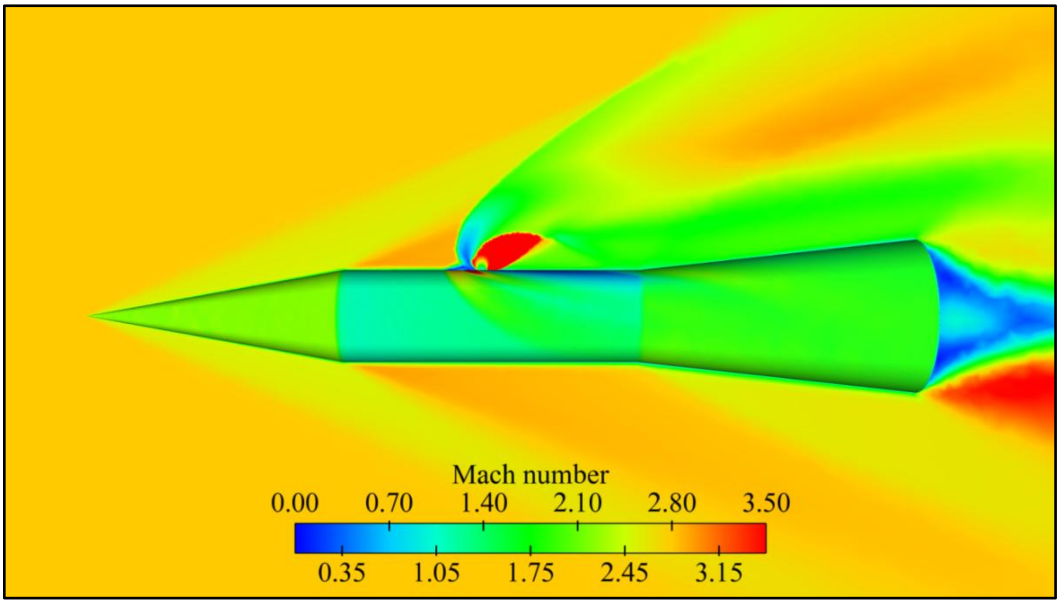

Figure 3-27: TM-2, Mach Number Distribution around the Model and Static Pressure Distribution on Model

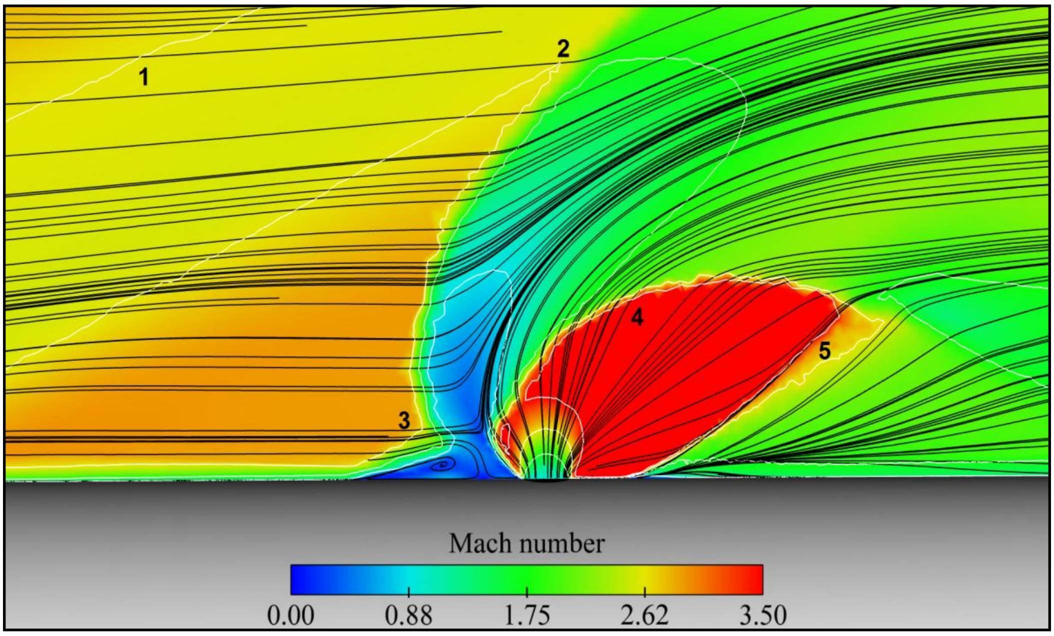

Figure 3-28: TM-2, Jet Exit Close-Up

3.3 Conclusions

In this part of the study, two missile-like geometries are used for validation of the numerical tools that are used in this thesis. For both models, experimental results and CFD results are in good agreement.

For TM-1, two configurations are tested at free stream Mach number of 2. In this test case, force and moment prediction capabilities of numerical tools are investigated. Errors between experimental data and numerical results are found to be acceptable. It is also verified that when the jet exit is placed near lifting surfaces, jet spread effects are denied by these lifting surfaces. Thus greater force amplifications are obtained. It is also verified that for negative angles of attack, force amplification decreases for both configurations, more notably for BT, due to jet wake being directed on the lifting surfaces, which are important contributors to the total normal force acting on the model. Greater interaction center of pressure values are obtained for BT, since tails are under effect of jet wake region and they have larger moment arm compared to canards in the other configuration. A turbulence model study is also conducted for TM-1. As a result of turbulence model study, k-ε model is found to more suitable to be used in the rest of thesis.

For TM-2, surface pressure prediction capabilities of the tools are investigated. It is also verified that as the roll angle increases, jet effects diminish. Flow structures are similar in both test cases, although free stream Mach numbers are different. As the result of this part of the thesis, a numerical approach has been validated for two supersonic test cases, which are missile like geometries with sonic lateral jet exits.

CHAPTER 4

PARAMETRIC STUDIES

For the remainder part of the study, a generic supersonic missile model will be used for investigation of jet effects for different jet parameters on pitch plane force and moment coefficients. The generic missile is called NASA-TCM [21] and is shown in Figure 4-1. Experimental data are available for free stream Mach number 1.75 and angles of attack between -4º and 24 º. It has an axisymetric body with 990 mm length and a maximum diameter of 66.04 mm. Nose is tangent ogive and it is 3 calibers in length. There are different canard and tail configurations. But it this study the configuration with identical canards and tails are investigated. Tails have 30º leading edge sweep angle, 59.4 mm semi span and 91.4 mm root chord. Missile is tested in “X” configuration in the wind tunnel.

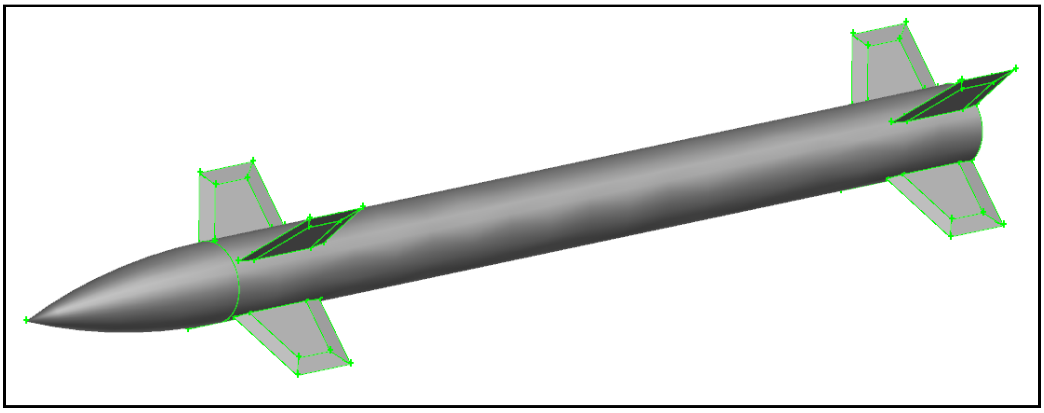

Figure 4-1: Isometric View of TCM

Firstly, no jet condition analysis will be made to verify the experiments. Experimental data are available for axial, normal force coefficient and pitching moment coefficient. . After this step, jet-exits will be inserted on the model for different locations. Jet-on simulations will be made for different parameters. 4 different jet locations are selected in pitch plane for jet exits. They are shown in below figure.

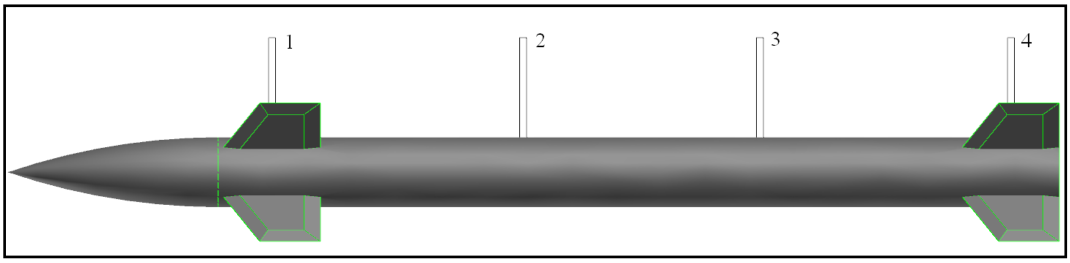

Figure 4-2: Jet Locations for TCM

Jet locations are placed 249 mm (1), 485 mm (2), 709 mm (3) and 945 mm (4) respectively from the nose tip. 1st and 4th jet locations are selected as the middle of root chords for canards and tails. 2nd jet location is the moment reference center for the missile.. Jet exit diameter is selected as 0.1 missile diameters as in two test models. 2 jet mass flow rates are selected as 0.2 kg/s and 0.4 kg/s and seven angles of attack are selected between -12° and 12° with 4° increments. Effects of these parameters on total missile force and moments as well as missile part force and moments will be investigated.

4.1 Jet-Off Validation Study

For validation of experiments, CFD analyses of NASA-TCM were made for free stream Mach number 1.75 and 5 angles of attack in absence of the jet. In Figures 4-3 to 4-5, experimental results are compared with CFD results for axial force, normal force and pitching moment coefficients. If these figures are examined, it can be seen that experimental and CFD results are in good agreement with each other. Maximum error is %10 for axial force coefficient. This may be probably due to mounting of a sting to the base of the model for wind tunnel experiments. It affects the base flow for the projectile. There is no such part in the CFD analysis and it is thought that most of the difference between two axial force coefficients comes from the base of the projectile.

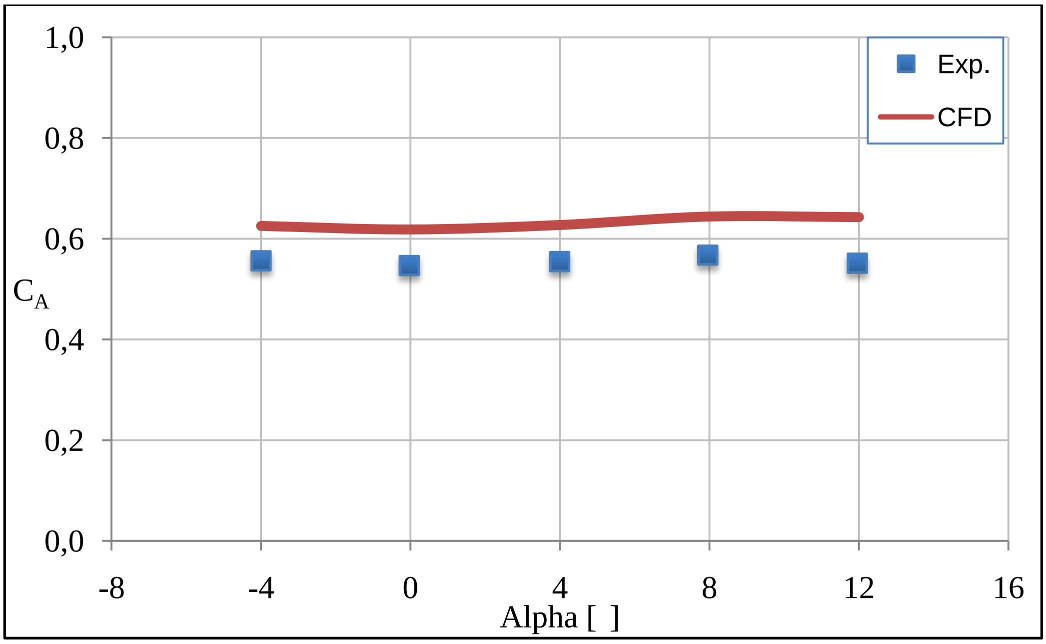

Figure 4-3: TCM, Axial Force Comparison

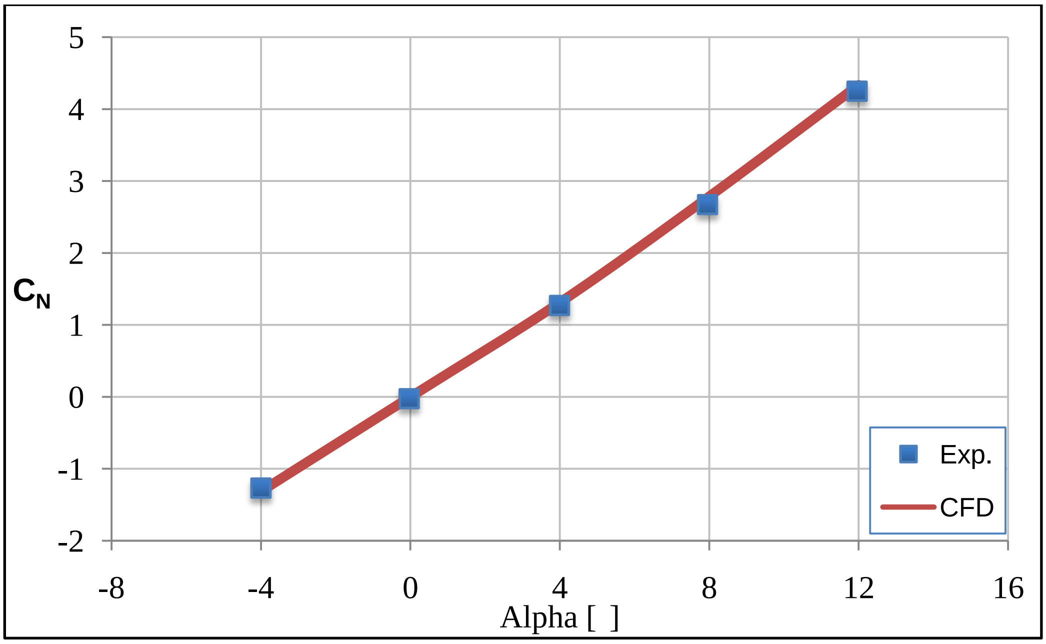

Figure 4-4: TCM, Normal Force Comparison

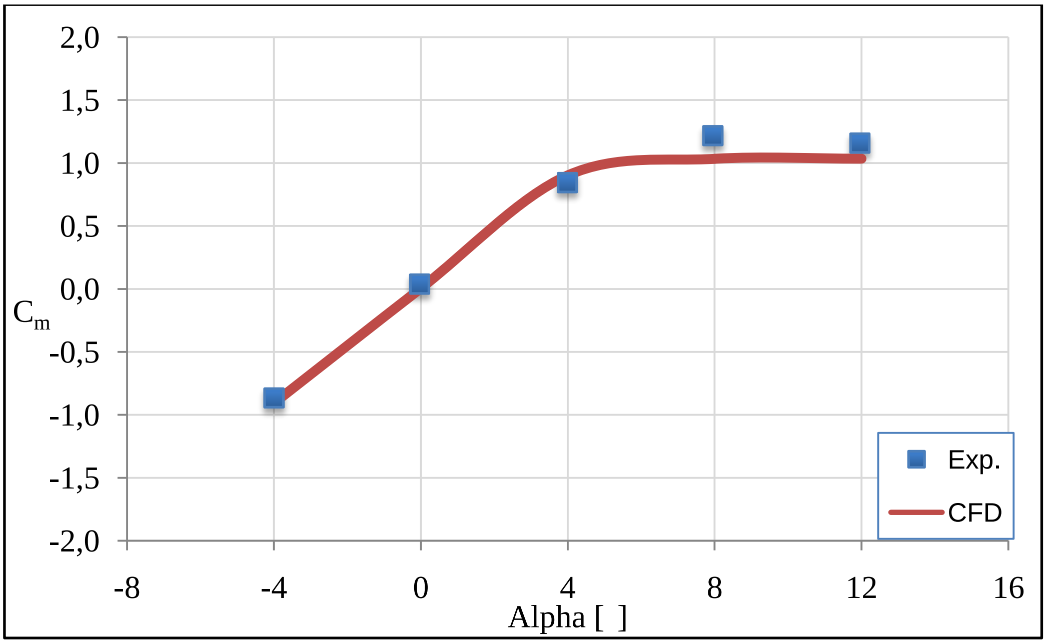

Figure 4-5: TCM, Pitching Moment Comparison

4.2 Grid Convergence Study

After jet-off validation part, next step is to analyze TCM with jet-on conditions. Before proceeding with the rest, a grid convergence study has to be made to minimize the errors concerning the quality of the grid. Grid Convergence study is conducted using jet location 4, jet mass flow rate 0.2 kg/s and -4º, 0º and 4º angles of attack. Coarse and fine grids are prepared, containing 3057917 and 4508359 cells for the half geometry. In TCM studies, since model shows symmetry about *x-z* axis, half model is prepared for time saving purposes. The grids prepared for this study are shown in Figure 4-6 and Figure 4-7. Analyses took approximately 7 and 11 hours respectively, in two nodes of a cluster. Each node has 4 processors and 4 gigabytes of random access memory per processor. Comparison of axial, normal force and pitching moment coefficients for two grids are shown in Table 4-1. Maximum difference between two grids is %2.7 percent for pitching moment coefficients. Considering the percent difference and running time, coarse grid is chosen for configuration 4 (x_{jet}= 0.945 m) and similar sized grids are used for other configurations.

Table 4-1: Grid Convergence Study Results

	Alpha [°]	C_A	C_N	C_m
Coarse Grid	-4	0,6496	-1,6731	1,5332
	0	0,6413	-0,3369	2,3021
	4	0,6533	0,9864	3,1351
Fine Grid	-4	0,6437	-1,6679	1,5311
	0	0,6343	-0,3329	2,2735
	4	0,6440	0,9952	3,0516
% Difference	-4	0,92	0,31	0,14
	0	1,08	1,21	1,25
	4	1,41	-0,89	2,66

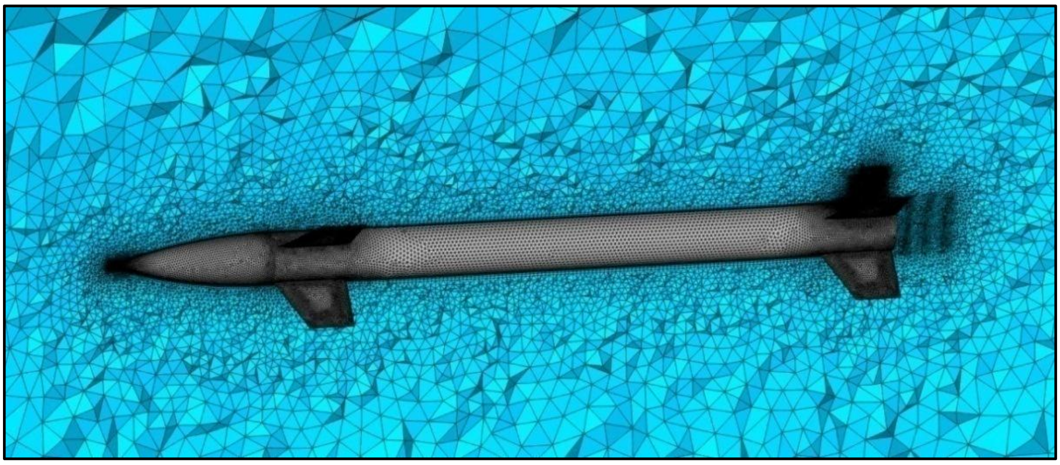

Figure 4-6: TCM Coarse Grid

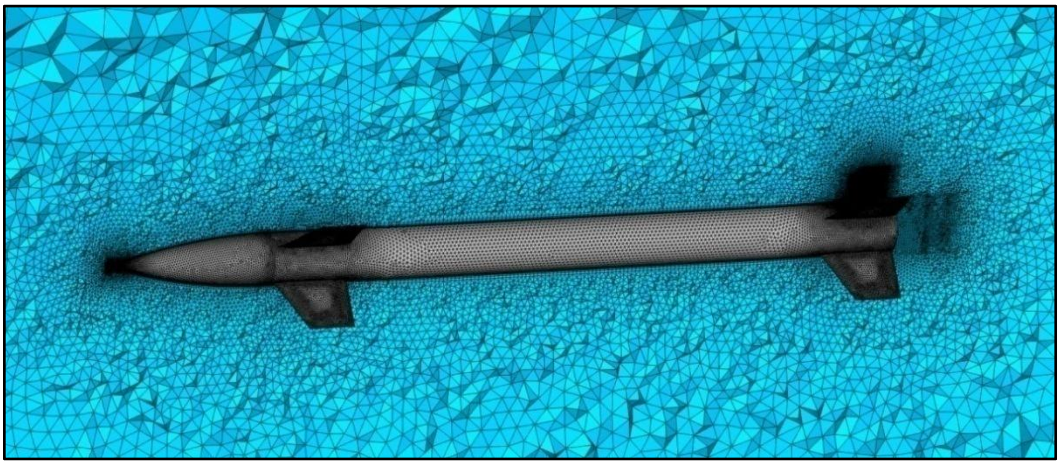

Figure 4-7: TCM Fine Grid

4.3 Results

CFD analyses are carried out for seven angles of attack, two jet mass flow inlet values and four jet locations. Depending on the location of the jet, configurations will be named C1, C2, C3 and C4, first being closest to nose tip. Test matrix is shown in Table 4-2.

Table 4-2: TCM Test Matrix

Mach Number	[1.75]
Angle of Attack [°]	[-12, -8, -4, 0, 4, 8, 12]
Jet Mass Flow Rate [kg/s]	[0.2, 0.4]
X_{jet} [m]	[0.249, 0.485, 0.709, 0.945]

As observed in Table 4-2, 56 CFD runs are carried out to determine how the variation of jet parameters affects the forces and moments on the whole missile and its components. Convention for the whole missile forces and moments has already been given in Figure 1-1. For tail and canard loads, convention is given in Figure 4-8. Convention is applicable to both tails and canards.

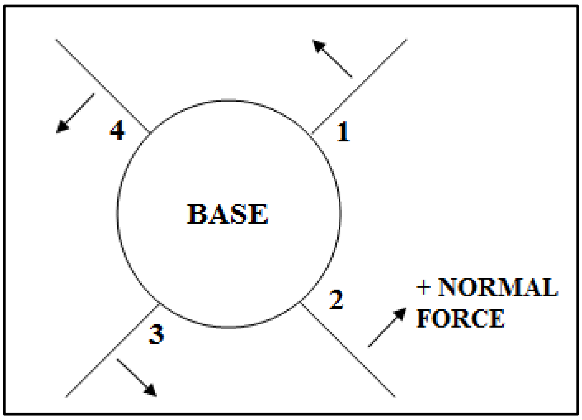

Figure 4-8: Lifting Surface Numbers and Normal Force Convention

Effects of jet parameters on missile force and coefficients are discussed in detail in the following parts.

Ambient and jet boundary conditions are given in Table 4-3.

Table 4-3: TCM Ambient and Jet Conditions

Ambient		Jet-1		Jet-2	
P[Pa]	54000	A[m^2]	3,43E-05	A[m^2]	3,43E-05
T[K]	255,7	mdot[kg/s]	0,4	mdot[kg/s]	0,2
M	1,75	M_{jet}	1	M_{jet}	1
U[m/s]	560,96	T_{jet}[K]	255,7	T_{jet}[K]	255,7
ρ[kg/m^3]	0,735745	T_{0jet}[K]	306,8	T_{0jet}[K]	306,8
L_{ref}[m]	0,06604	U[m/s]	320,55	U[m/s]	320,55
A_{ref}[m^2]	0,0034253	P[Pa]	2673777	P[Pa]	1336888

4.3.1 Total Normal Force Coefficient

Effects of jet parameters on total missile normal force coefficient are shown in Figure 4-9. The legend used in this figure is used for all following figures in the remaining sub sections of Chapter 4-3. In these figures, black solid line represent no-jet condition, naval blue line represents C1, red line represents C2, green line represents C3 and brown line represents C4. For C1 to C4, solid lines represent 0.2 kg/s mass flow rate and dashed lines represent 0.4 kg/s mass flow rate.

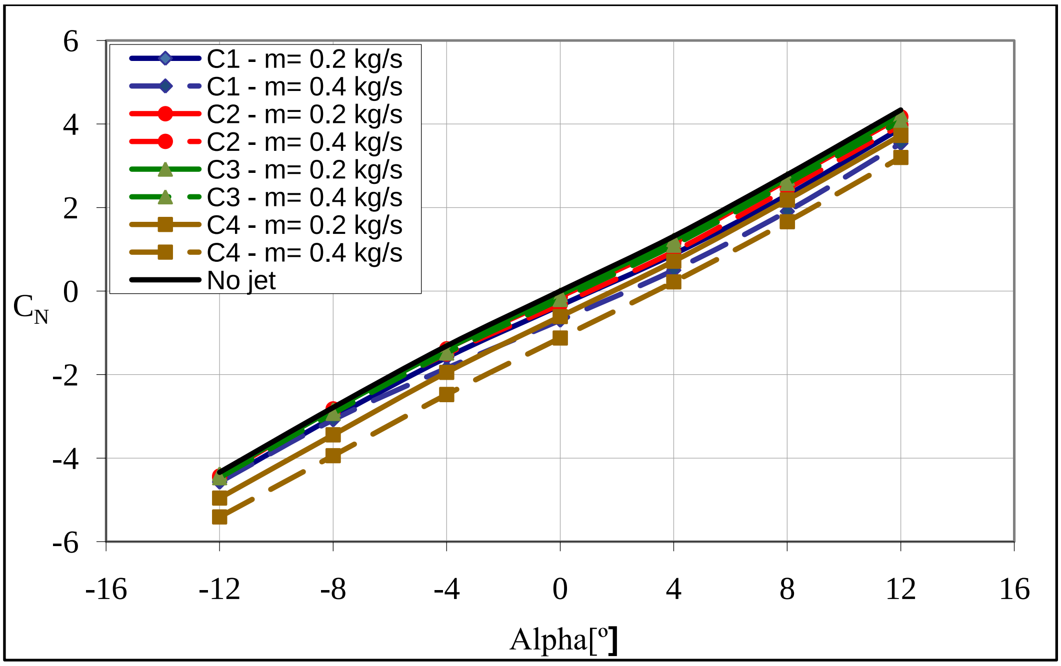

Figure 4-9: TCM-Variation of Total Normal Force With Jet Parameters

If Figure 4-9 is examined, in C1 and C4, the configurations in which jet exits are located between lifting surfaces, jet effects are more observable. Jet alone creates normal force in -C_N direction. C_N curve shifts downwards more in C1 and C4 since already stated in TM-1 results, canards and tails block the wrap around effect of the jet interaction region. In these configurations, lifting surfaces are directly affected by the presence of the jet. Pressure in the upper surfaces of canards and tails increases due to the jet exit, their contribution to total normal force also increases. In C2 and C3, low pressure region on the body is spread to larger regions on the body. In these configurations, jet effect and low pressure upper zone which causes a force in direction of C_N, cancel out each other.

4.3.2 Pitching Moment Coefficient

Effects of jet parameters on total missile pitching moment coefficient are shown in Figure 4-10. Moment center is 0.485 m from the nose tip.

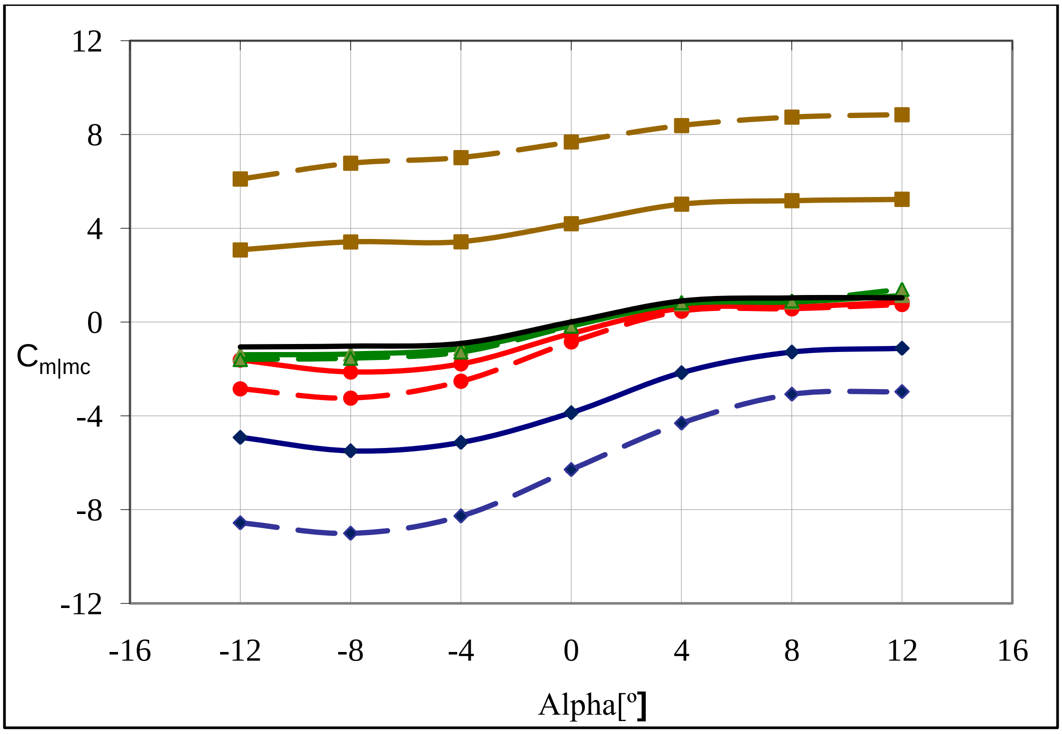

Figure 4-10: TCM-Variation of Pitching Moment with Jet Parameters

In Figure 4-10, it is clearly observed that placing the jet exit in front of the moment reference center, C1, yields the moment curve to shift downwards. Upward ejecting jet creates a pitch down moment and according to Figure 1-1 in C1. Opposite to that, placing the jet behind the moment reference center, C4, enhances a pitch up moment and shifts the curve downwards. In C1 and C4, increasing the mass flow rate increases the magnitudes of pitching moments. For these two configurations, jet acts like deflected control surfaces. Pitching moment values are nearly four times higher than no jet configurations. For C2 and C3, moment gain is less than former configurations. In C3, moment variation with jet parameters is the least significant. For C2, moment couple which is formed around the moment center due to upstream high pressure and downstream low pressure is more visible.

4.3.3 Force Amplification Factor

Effects of jet parameters on force amplification factor *K* are shown in Figure 4-11.

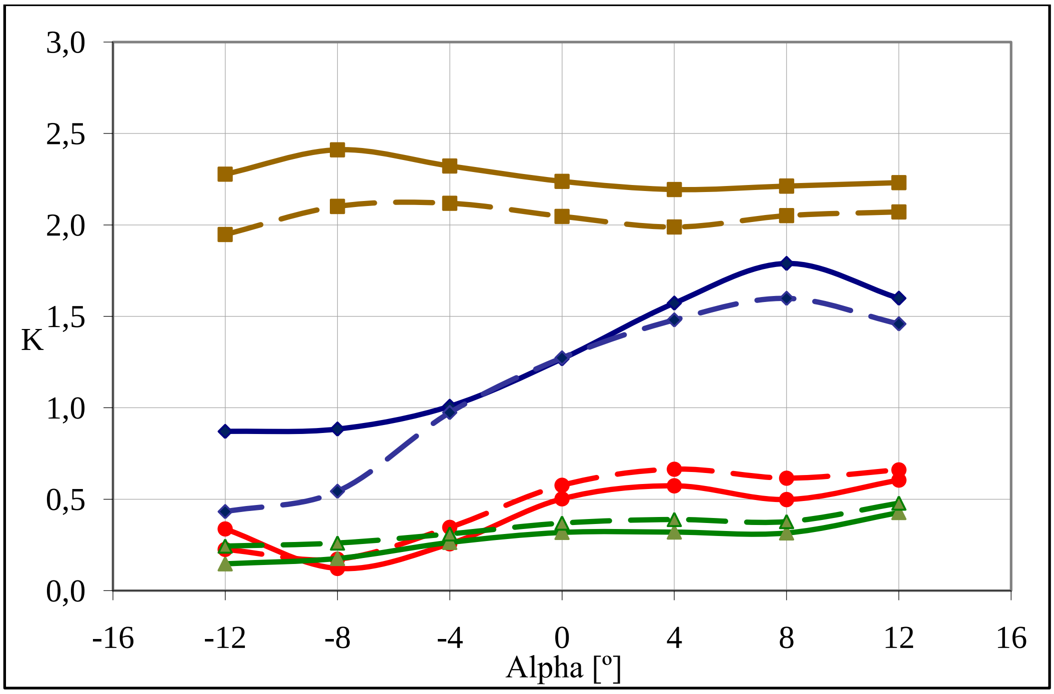

Figure 4-11: TCM-Variation of Force Amplification Factor with Jet Parameters

For *K* values, in C2 and C3 values are less than unity in entire angle of attack range. In these configurations jet exits are located between the lifting surfaces. As mentioned previously in TM-1 studies; strong shocks, separation zones are effective in larger body areas in C2-C3 than C1-C4. Thus surface pressure distribution is more severely affected and force amplification is lower due to larger interaction areas. Larger interactions areas mean more low pressure zones on the body. Also for these configurations, force amplification increases with increasing angle of attack as in TM-1 for BT configuration. In C4, since jet is located very close to aft of the body, effected body area is less and *K* values are much higher. In C1 for low angles of attack, *K* values are less than unity. As in C4, in C1 jet is also surrounded by lifting surface but *K* values are less than unity in negative angles of attack. For C2 and C3, force amplification increases with increasing mass flow rate but for the remaining configurations, there is no direct relation.

4.3.4 Axial Force Coefficient

Effects of jet parameters on axial force coefficient are shown in Figure 4-12.

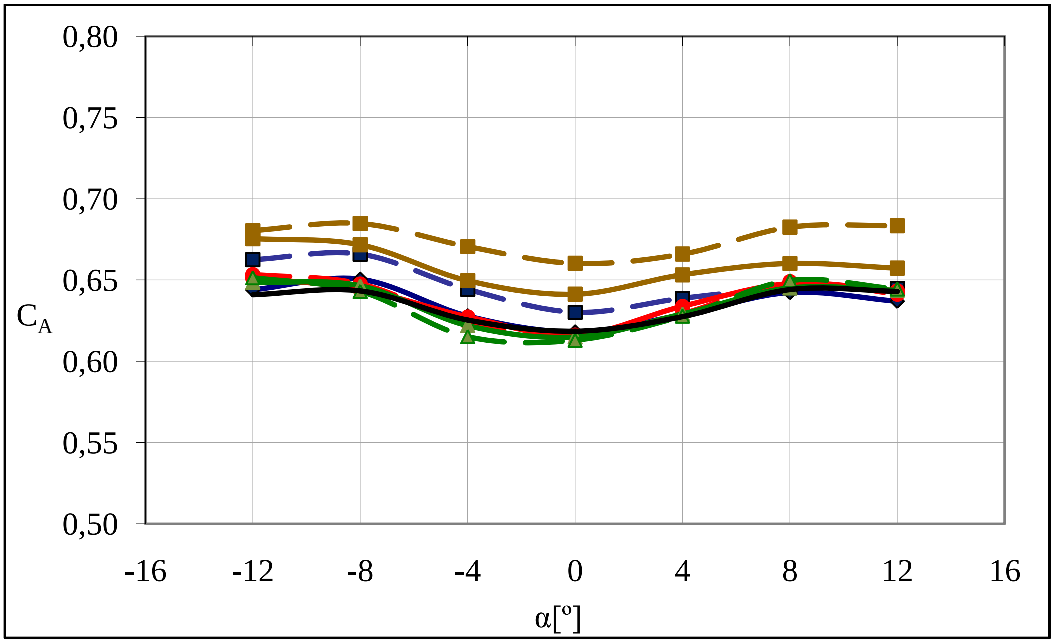

Figure 4-12: TCM-Variation of Axial Force Coefficient with Jet Parameters

Variation of axial force is important since it may be necessary for thruster requirements of the missile. In Figure 4-12, axial force increases considerably in C4, where jet exit is closest to the base of the projectile. Extra base drag is produced in this case, where jet blocks the oncoming flow and decreases the pressure at the base of the missile. There is also slight increase for negative angles of attack in C1, and this increase is due to increase in the axial force of the lifting surfaces, which are located near to jet exit. Tail or canard axial forces increase with mass flow rate. Axial force shows no significant variation in C2 or C3.

4.3.5 Canard-3 Normal Force Coefficient

Effects of jet parameters on Canard-3 normal force coefficient are shown in Figure 4-13.

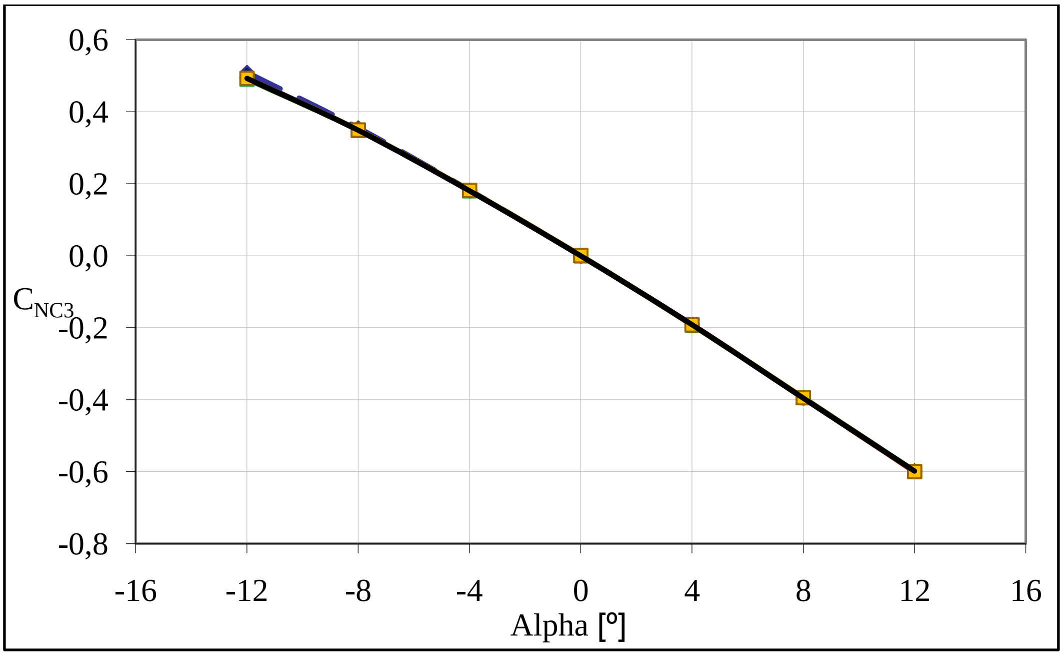

Figure 4-13: TCM-Variation of Canard-3 Normal Force Coefficient with Jet Parameters

If Figure 4-13 is examined, it can be seen that normal force on canard-3 is entirely unaffected by the presence of the jet. It is located on lower half of the missile and jet locations are on the upper half. Jet effects do not reach Canard-3 and variation of Canard-3 normal force with angle of attack is the same as no-jet case.

4.3.6 Canard-4 Normal Force Coefficient

Effects of jet parameters on Canard-4 normal force coefficient are shown in Figure 4-14.

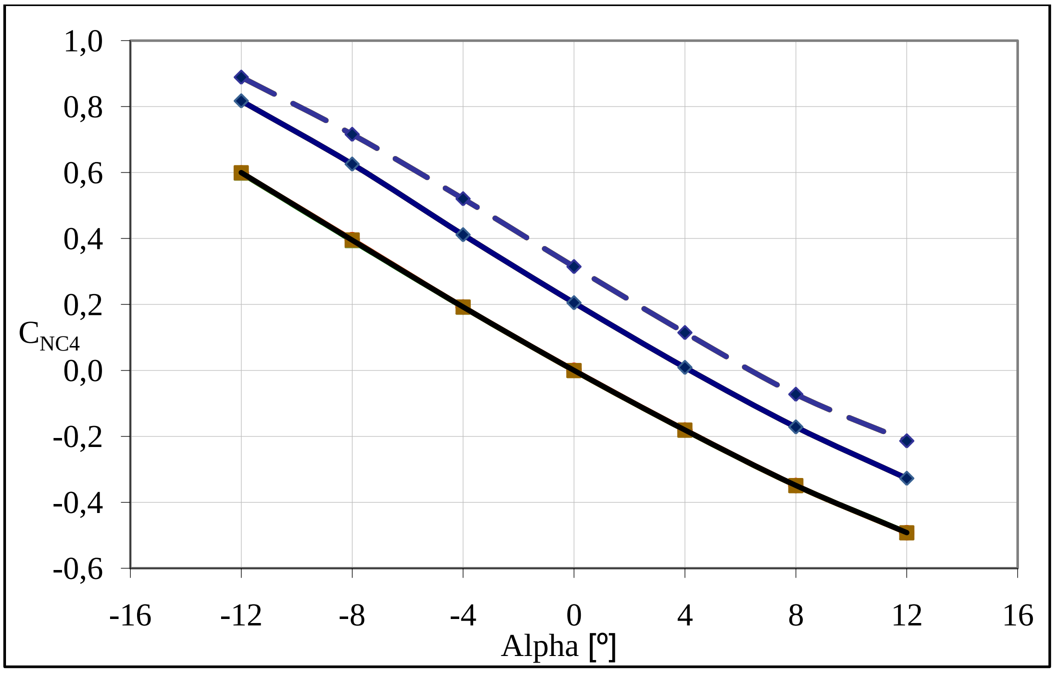

Figure 4-14: TCM-Variation of Canard-4 Normal force Coefficient with Jet Parameters

For C2, C3 and C4, canard normal force is not affected by the presence of the jet. But jet normal force is affected in C1 obviously. In this configuration, jet is placed in the midpoint of root chord of Canard-4. High pressure zone caused by the jet affects the near placed canards and increases the magnitude of the normal force. Normal force on a lifting surface is created by the pressure difference between its upper and lower surfaces. Presence of the jet increases the pressure on the upper surface of Canard-4 and normal force is increased according to Figure 4-8. As mass flow rate increases, pressure also increases and the curve shifts further upwards as expected. An important conclusion can be made from Figure 4-14. Jet effects begin to diminish for upstream zones on the missile body as the jet location moves to further aft of the body. For C2 to C4, Canard-4 is not affected and the variation is the same as no-jet case.

4.3.7 Tail-3 Normal Force Coefficient

Effects of jet parameters on Tail-3 normal force coefficient are shown in Figure 4-15.

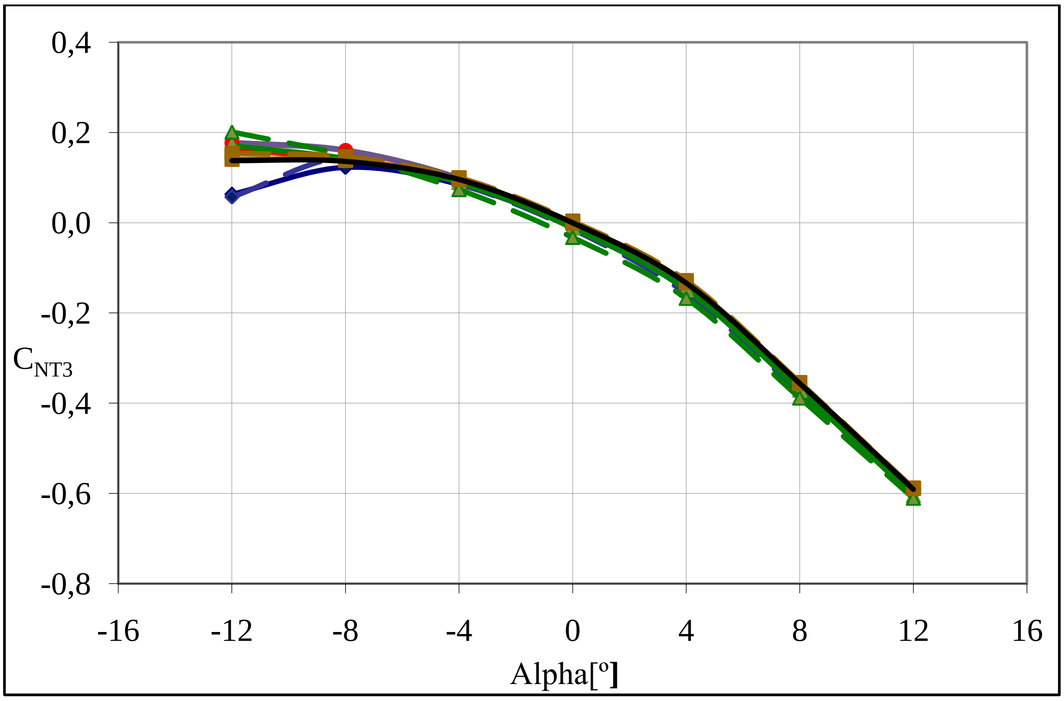

Figure 4-15: TCM-Variation of Tail-3 Normal Force Coefficient with Jet Parameters

Variation of Tail-3 normal force with jet parameters is similar to variation of Canard -3 normal force with jet parameters. General trend of the curve is similar to no-jet case. Like Canard 3, Tail-3 is placed on the lower half. Slight decrease in magnitude of normal force in negative angles of attack is observed for C1. In this zone, jet wake is directed downwards due to negative component of velocity vector. Tail 3 is affected by directed wake flow and wake vortices, pressure on the upper surface of Tail-3 decreases thus creating a loss in the normal force of Tail-3.

4.3.8 Tail -4 Normal Force Coefficient

Effects of jet parameters on Tail-4 normal force coefficient are shown in Figure 4-16

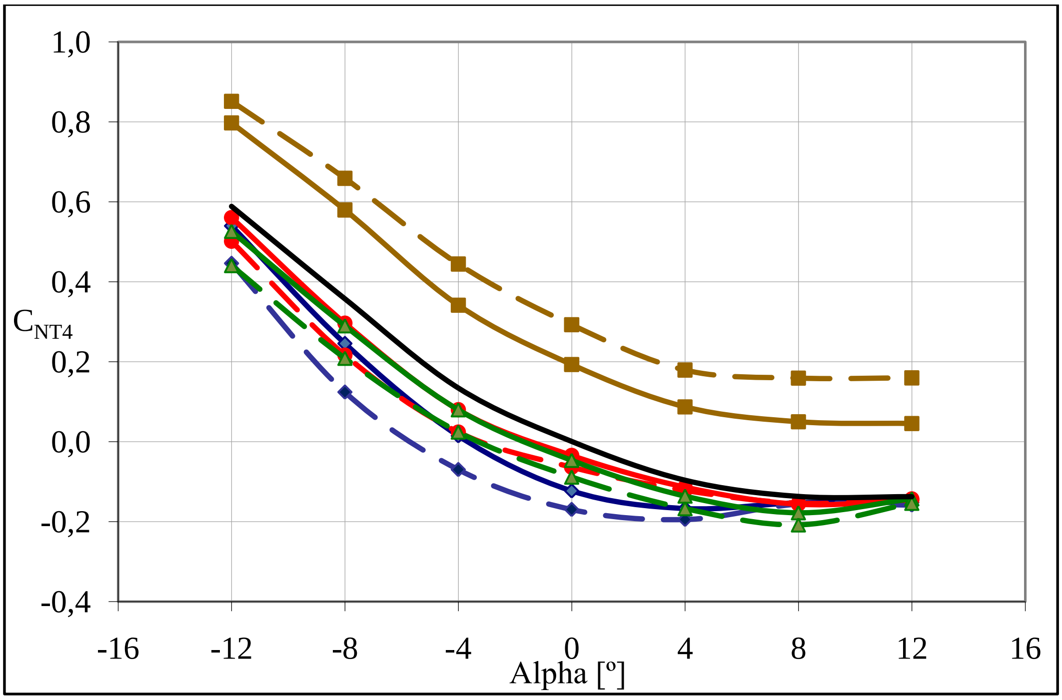

Figure 4-16: TCM-Variation of Tail 4 Normal Force with Jet Parameters

If above figure is examined, it may be seen that downstream influence zone for the jet exit is so large that even in C1; tail normal force is affected by the jet interaction. In C4, jet effects are more visible since in that configuration, jet is located in the vicinity of Tail 4. Tail-4 normal force for C4 is similar to Canard-4 normal force for C1. Jet normal force is in negative sense; since the upper part of Tail 4 is affected from the high pressure fluid, it also has extra negative normal force. Normal force for C4 increases with increasing mass flow rate. For other configurations, Tail-4 normal force is affected more visibly in negative angles of attack, as the jet flow is directed onto Tail-4 in this zone.

If Figure 4-14 and Figure 4-16 are examined together, an important conclusion can be drawn. Downstream influence zone of the jet is larger than upstream influence zone. Both Tail-4 and Canard-4 are located on the upper half of the missile with jets. For Canard-3, normal force is only affected in C1 where the jet exit is located in the vicinity of Canard-4 whereas Tail 4 is affected in all configurations. In the Figures 4-17 to 4-19, upper half surface pressure distributions of TCM for different jet locations are shown comparatively.

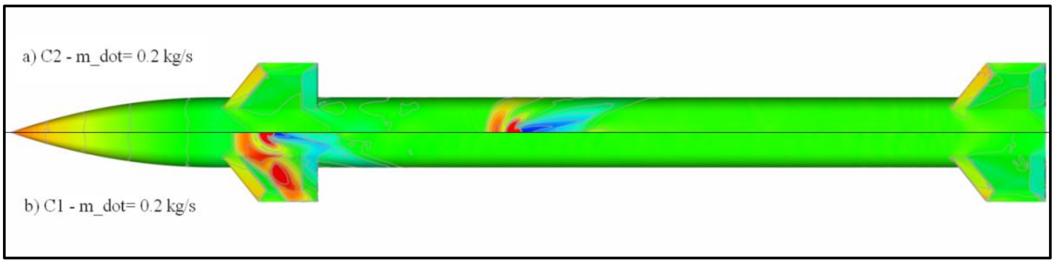

Figure 4-17: TCM-Surface Pressure Distribution, a) C2 α= 0°, $\dot{m}$= 0.2 kg/s, b) C1, α= 0°, $\dot{m}$= 0.2 kg/s

Figure 4-18: TCM-Surface Pressure Distribution, a) C3 α= 0°, $\dot{m}$= 0.2 kg/s, b) C1, α= 0°, $\dot{m}$= 0.2 kg/s

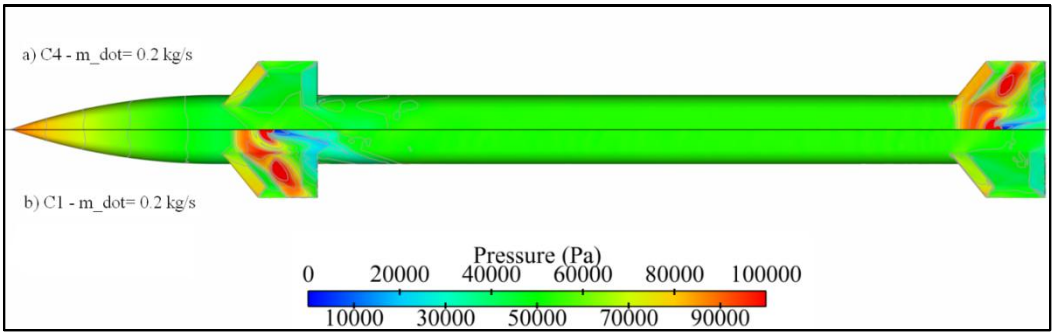

Figure 4-19: TCM-Surface Pressure Distribution, a) C4 α= 0°, $\dot{m}$= 0.2 kg/s, b) C1, α= 0°, $\dot{m}$= 0.2 kg/s

In above figures, it may be observed that jet upstream pressure distributions for C2, C3 and C4 are similar to each other. Even for C1, pressure distribution on nose is similar to other configurations. But if Tail 4 pressure distributions are examined, they are different from each other. Jet effects extend to tails which are located at the base of the missile, even for C1. Disturbed flow field decreases pressure on the upper surfaces of tails thus Tail-4 the normal forces. In Figure 4-20 and Figure 4-21, C1 and C4 surface pressure distributions are compared with no jet condition case. In these figures, it is also evident that upstream pressure distributions are also very similar to no jet case. But Tail 4 pressure distributions are different with respect to each other and to no jet case. I t should be noted that all figures for surface pressure distributions share the same legend with Figure 4-19.

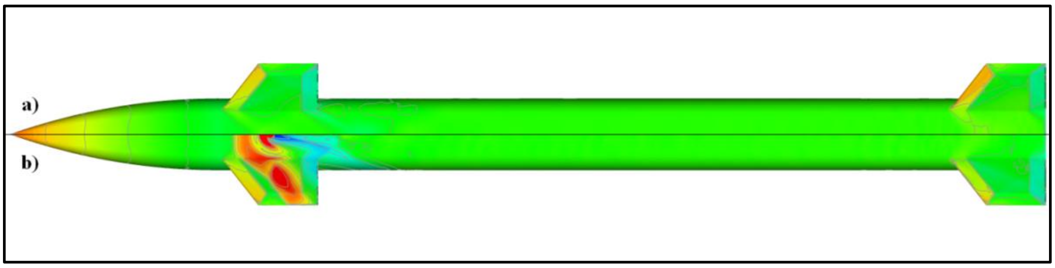

Figure 4-20: TCM-Surface Pressure Distribution, a) No jet, α= 0°b) C1, α= 0°, $\dot{m}$= 0.2 kg/s

Figure 4-21: TCM Surface Pressure Distribution, a) No jet, α= 0°b) C4, α= 0°, $\dot{m}$= 0.2 kg/s

In Figure 4-22, a detailed picture for Tail-4 pressure distribution is shown for C1 in comparison with no jet condition. C1 has the maximum jet location distance with respect to Tail 4. But if surface pressures are compared, there are differences mostly in the leading edge section. Tail-4 in C1 has lower pressure compared to no jet condition. It can be stated that jet wake influence zone which causes pressure decrease is present even 10 diameters downstream of the jet exit.

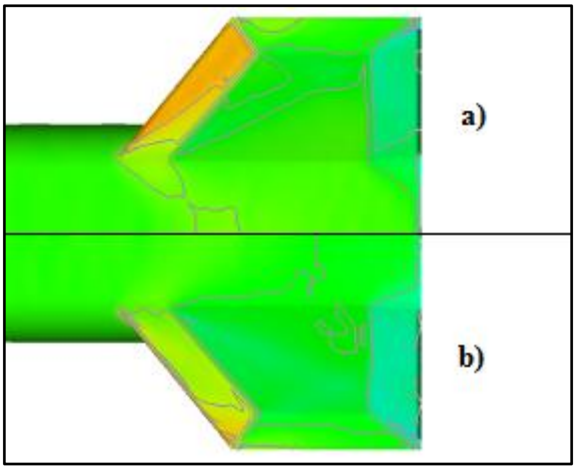

Figure 4-22: TCM-Tail 4 Surface Pressure Distribution, a) No jet, α= 0°b) C1, α= 0°, $\dot{m}$= 0.2 kg/s

In Figure 4-23, surface pressure distribution for two mass flow rates are compared for C1. In this figure, it is evident that increasing the mass flow rate increases the upstream influence zone area. Surface pressure on Canard-4 is increased more in 0.4 kg/s mass flow rate case. But in the nose section surface pressure distribution is similar to each other for two cases. It is also interesting to see that increasing the mass flow rate has little effect on downstream pressure distribution. Strength of the downstream separation zone has increased in 0.4 kg /s case but Tail-4 pressure distribution is also similar to each other.

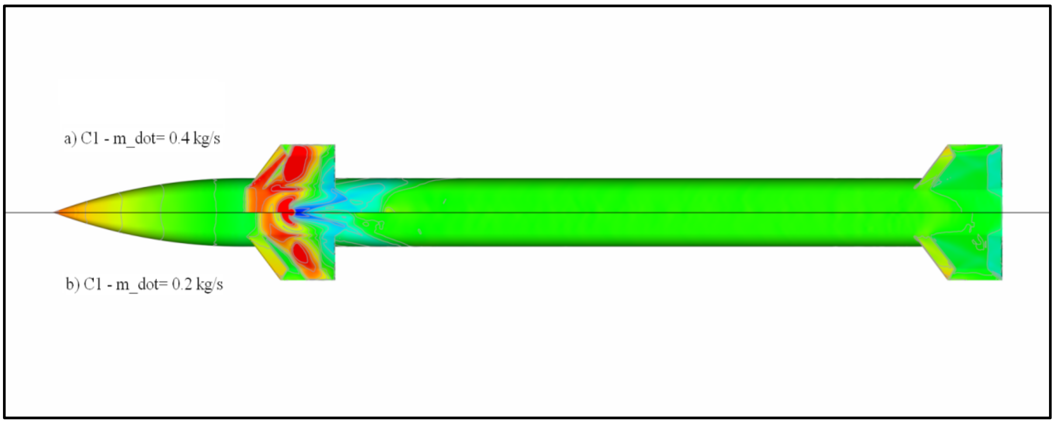

Figure 4-23: TCM C1 Surface Pressure Distribution, a) $\dot{m}$= 0.4 kg/s, α= 0°b), α= 0°, $\dot{m}$= 0.2 kg/s

4.4 Comparison of Deflected Tail and C4 Jet Cases

As it was discussed in the beginning of the thesis, lateral jet control is an alternative to control surface deflection for missile maneuver control. A comparative study is conducted for TCM for -5º and -10º tail pitch deflections and 4th configuration with two mass flow rates. In this study, hinge line of the tails is selected 45 mm from the root chord leading edge. Comparative results are shown in following figures for normal force and pitching moment. Deflection axis for tails lies on spanwise plane, it is directed away from the centerline of the missile and deflection obeys right hand rule. In Figure 1-3, positive tail pitch deflection can be seen.

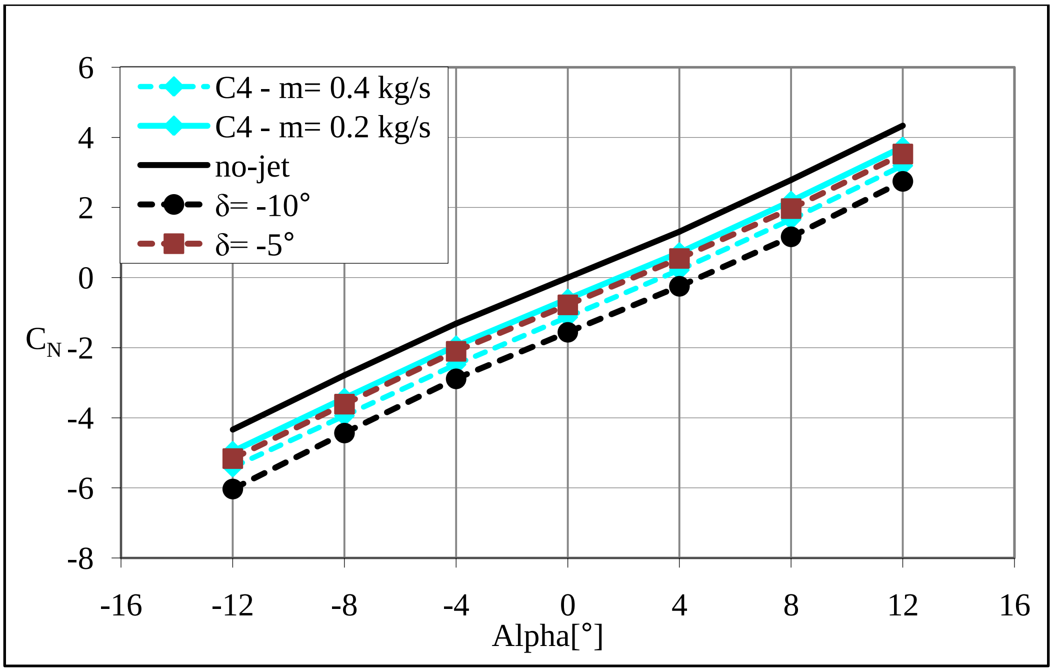

Figure 4-24: TCM , Normal Force Comparison of Tail Deflection and C4 Jet Cases

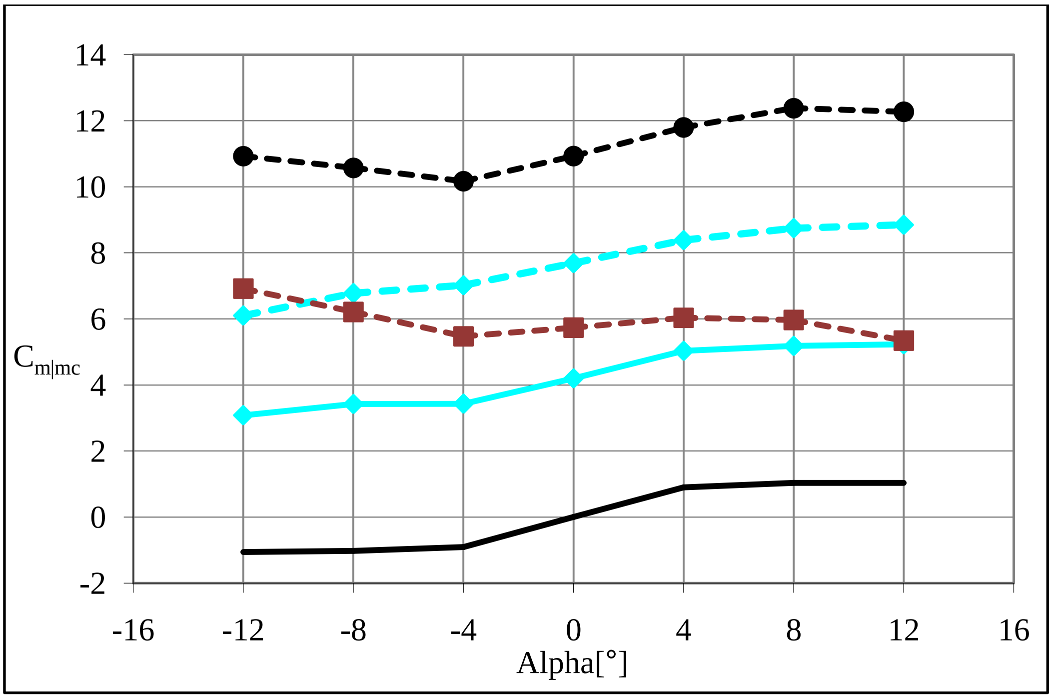

Figure 4-25: TCM, Pitching Moment Comparison of Tail Deflection and C4 Jet Cases

If above figures are examined, jet control and surface deflection control behave in similar ways for force and moment coefficients. 0.4 kg/s mass flow rate case lies between -5º and -10º pitch deflection curves. For deflection cases, as deflection angle increases, normal force and pitching moment acting on the missile also increases. It is similar situation for jet case. As jet mass flow rate is increases, force and moment on the missile also increases. For the cases used in this study, 0.4 kg/s mass flow rate sonic jet located between tails shows similar impact on the missile for a tail pitch deflection value between -5º and -10º.

4.5 Conclusions

In this chapter, a parametric study for a generic supersonic missile with lateral jet injection is conducted. Total 56 jet-on CFD runs were conducted and results are comparatively shown in graphs and surface pressure contours.

As found in TM-1 [14], greater force amplification factors are obtained for the configurations where the jet exit is located between the lifting surfaces. For C1 and C4, force amplification factors are generally greater than 1, as found by several authors in literature [14][20][32], when the jet is located between a pair of lifting surfaces. For C2 and C3, jet wraparound effect cannot be blocked by the lifting surfaces and downstream low pressure zone is more dominant. Also in C1 and C4, upper lifting surface pressures are increased by the presence of the jet thus enhancing further force amplification. It is also verified for negative angles of attack, jet wake is directed to tails and force amplification decreases.

Total pitching moment acting on the missile increases when jet locations have large moment arms as in C1 and C4. Pitching moment is further increased when jet mass flow rate is increased from 0.2 to 0.4 kg/s.

Another important conclusion to be drawn from this chapter is that downstream of the jet is affected more than the upstream of the jet. If lifting surface normal forces and pressure distributions are examined; when the jet is placed further downstream than C1, upstream effects begin to diminish for canards. But the presence of the jet is visible in Tail 4 even when jet is located between canards (C1). It is also found out that conventional control and lateral jet control have similar affects on missile force and moments.

CHAPTER 5

CONCLUSIONS AND FUTURE WORK

In this study, lateral jet controlled missile aerodynamics was studied numerically by using the commercial CFD software FLUENT. The study is mainly divided into three parts; governing equations and flow physics, test case validations and parametric studies.

In the first part, governing equations of compressible and viscous fluid motion are stated. They are three fundamental conservation equations. Auxiliary equations, which are to be used for calculation of boundary conditions, are introduced. Prominent flow features for the ejection of high speed jet into supersonic stream are stated by the help of work done in literature. Commercial software to be used in the study is explained. Equation discretization and numerical models are also given in this chapter.

Numerical validation studies are conducted using two test cases of which experimental data are available. Test cases are missile like geometries which are tested in supersonic free stream and with sonic lateral jets located on the body in wind tunnels. For Test Model-1, turbulence model study is conducted. CFD results using two different turbulence models agreed well with experimental data. As a result k-ε turbulence model is selected by considering the agreement with experimental data, CPU time and ease of convergence.

TM-1 studies are carried out by using two different configurations; Body-Canard and Body-Tail. Results showed that greater force amplification factors are obtained when the jet exit is located between lifting surfaces, which deny the wrap around effect of the jet interaction region for an axisymmetric body. It was also verified that for negative angles of attack, jet wake is directed onto lifting surfaces and reduction in force amplification is observed. For both configurations, CFD results agreed well with experimental data.

For TM-2, surface pressure coefficients calculated from CFD are compared with experimentally reported coefficients for three different roll angles. Differences between calculated and reported results were in acceptable margin. Flow over the vicinity of the jet is examined separately for this model and it was seen that important flow features such as shocks and separation regions are captured by the CFD simulations. After two test case studies, a numerical methodology has been verified for lateral jet controlled supersonic missile problems.

For parametric studies, a generic supersonic missile shape, TCM, is selected. Experimental data for TCM is available so that another tool validation for jet-off TCM experiments is conducted. After this step, four jet locations are determined and jet-on CFD runs are made for TCM for four jet locations, two mass flow rates and seven angles of attack. Behaviors of lifting surface normal forces, total normal force and pitching moment of the missile are investigated for different jet parameters.

Important conclusions are made after parametric studies. It was verified that force amplification is larger when the jet is between lifting surfaces, as it was the case in TM-1. Pitching moment acting on the total missile configuration greatly increased when jet is either between canards or tails. Magnitude of normal force also increased from no-jet case for C1 and C4. Also it was found out that downstream influence zone of the jet exit is larger than the upstream influence zone of the jet. Comparative figures for different configurations also supported this statement. An increase in axial force is also observed when jet exit is located closer to the base of the missile.

For future work, more advanced turbulence modeling is planned for lateral jet controlled missile problems. With advances in computing technology it may be possible in near future to perform CFD calculations with LES or DES simulations for high Reynolds number flows with mesh numbers equal to models in this study for feasible running times.

Numerical lateral jet controlled missile problems are solved in hypersonic regime by several authors [14]. It is planned to find out whether the techniques and procedure used in this study is applicable to hypersonic regime problems or not. Also time dependent phenomena for jet interaction case will be investigated. Another target is to find the effect of jet-exit temperature to overall jet controlled missile aerodynamics. Combined effect of two orthogonal jets on a missile will also be investigated.

As the result of the parametric studies, a database is generated. In this database, missile force and moment coefficients with respect to jet parameters are included. This database will be enlarged, with different Mach numbers and different jet pressures. It is planned to build a fast prediction side jet design tool which can be used for initial design steps of total missile configuration design. Interference factors will be introduced for missile components such as body, nose and lifting surfaces. These interference factors will be a measure of the difference between jet on and jet off cases for a missile component. Like the component build up technique, a jet design tool will be developed. This tool will take jet off missile component force and moment coefficients, then by using the interference factors, jet on force and moment coefficients will be predicted without doing CFD simulations.

REFERENCES

[1] Fleeman, E., L, “Tactical Missile Design”, AIAA Education Series, 2001

[2] Erdem, E., “Thrust Vector Control By Secondary Injection”, Master Thesis, METU, 2006

[3] Graham, M., J., Weinacht, P.,” Numerical Investigation of Supersonic Jet Interaction for Axisymetric Bodies”, AIAA Journal of Spacecraft and Rockets, Vol.37, No.5, 2000, pp.675-683

[4] Cassel, L., A., “Applying Jet Interaction Technology”, AIAA Journal of Spacecraft and Rockets, Vol.40, No.4, 2003, pp.523-637

[5] Srivastava, B.,” Computational Analysis and Validation Studies for Lateral Jet Controlled Missiles”, AIAA Journal of Spacecraft and Rockets, Vol.34, No.5, 1997, pp.584-592

[6] Anderson, J., D., “Fundamentals of Aerodynamics”, McGraw and Hill, 2001

[7] Gnemmi, P., Adeli., R., Longo, J., “Computational Comparison of the Interaction of a Lateral Jet on a Supersonic Generic Missile”, AIAA Atmospheric Flight Mechanics Conference and Exhibit, 2008,

[8] Designation Systems: http://www.designation-systems.net/dusrm/m-166.html, Last visited on August 2011

[9] Designation Systems: http://www.designation-systems.net/dusrm/thaad.html, Last visited on August 2011

[10] Lockheed Martin: http://www.lockheedmartin.com/products/thaad/, Last visited on August 2011

[11] Designation Systems: http://www.designation-systems.net/dusrm/app4/ pac-3.html, Last visited on August 2011

[12] Lockheed-Martin:http://www.lockheedmartin.com/products/PAC-3/index. Html, Last visited on August 2011

[13] Orth, R., C., Funk, J., A., "An Experimental and Comparative Study of Jet Penetration in Supersonic Flow", AIAA Journal of Spacecraft, Vol.4, No.9, 1967, pp.1236-1242

[14] Brandeis, J., Gill, J., "Experimental Investigation of Super and Hypersonic Jet Interaction on Missile Configurations" , AIAA Journal of Spacecraft and Rockets, Vol.35, No.3, 1998, pp.296-302

[15] Schetz, J., A., "Interaction Shock Shape for Transverse Injection in Supersonic Flow", AIAA Journal of Spacecraft, Vol.7, No.2, 1970, pp.143-149

[16] Werle, M., J., Driftmyer, R., T., Shaffer, D., G., "Jet Interaction Induces Separation: Two Dimensional Problem", AIAA Journal, Vol.10, No.2, 1967, pp.188-193

[17] Lee, J., W., Min, B., Byun, Y., Lee, C., "Numerical Analysis and Design Optimization of Lateral Jet Controlled Missiles", ICTAM04 Proceedings

[18] Higgins, K., Schmidt, S., “Simulation of a Sonic Jet Injected to A Supersonic Cross Flow”, 16th Australasian Fluid Mechanics Conference, 2007, pp.608-612

[19] Kovar, A., Schülein, E., “Comparison of Experimental and Numerical Investigation of a Jet In a Supersonic Cross Flow”, The Aeronautical Journal, 2006, pp.353-360

[20] DeSpirito, J., “Factors Affecting Reaction Jet Interaction Effects on Projectiles”, 29th AIAA Applied Aerodynamics Conference, 2011,

[21] “Assessment of Turbulence Modeling for High Speed Vehicles”, NATO-RTO Technical Report, 2005

[22] White, F., M., “Viscous Fluid Flow”, McGraw and Hill, 1991

[23] “FLUENT Theory Guide”, ANSYS, 2009

[24] Anderson, J., D., “Modern Compressible Flow”, McGraw and Hill, 1991

[25] Zucker, R., D., Biblarz, O., “Fundamentals of Gas Dynamics”, John Wiley and Sons, 2002

[26] Spaid, F., W., Cassel, L., “Aerodynamic Interference Induced by Reaction Controls”, AGARDograph No.173, 1973

[27] Brandeis, J., Gill, J., “Experimental Investigation of Side-Jet Steering for Supersonic and Hypersonic Missiles” , AIAA Journal of Spacecraft and Rockets, Vol.33, No.3, 1996, pp.346-352

[28] Wilcox, D., C., “Turbulence Modeling for CFD”, DCW Industries, 2010

[29] Gerasimov, A., “Modeling Turbulent Flows with Fluent”, FLUENT Webinar, 2006

[30] Hoffmann, K., A., Chang, S.,T., “Computational Fluid Dynamics Volume III”, Engineering Education System, 2000

[31] Salim, M., S., Cheah, S., C., “ Wall y^+ Strategy for Dealing with Wall-Bounded Turnulent Flows”, IMECS, 2009

[32] Graham, M., J., Weinacht, P., Brandeis, J., Angelini, R., “A Numerical Investigation for Supersonic Jet Interaction for Finned Bodies”, ARL Technical Report 2312, 2000

[33] Gilman, B., G., “Control Jet Interaction Investigation”, AIAA Journal of Spacecraft, Vol.8, No.4, 1971, pp.334-339

APPENDIX

TEST MODEL-1 CALCULATIONS

In this section, calculation of boundary conditions for Test Model 1 CFD simulations is given in detail. Similar procedure is applied to TM-2 and TCM simulations.

In FLUENT, *Pressure-Far-Field* boundary condition is defined for external flow domain. In this type, free stream static pressure, static temperature and Mach number is given as inputs. In the reference wind tunnel experiment [14], wind tunnel stagnation pressure, temperature and Mach number is given. Static properties are calculated from Equations (2-8) and (2-9). Calculated static values are given in Table A-1. Turbulence specification is selected as default type k-ε with default values.

Table A-1: TM-1-BC Static Free Stream Boundary Conditions

M_∞	$P_{0\infty}$[kg/cm^2]	$P_{0\infty}$[Pa]	$P_{s\infty}$[Pa]	$T_{0\infty}$[K]	$T_{S\infty}$[K]
2	1,95	191295	24721,2	306	170

Jet exits are defined as *Mass Flow Inlet.* In this type, static pressure, stagnation temperature and mass flow rate is required to define the flow. In the reference, jet stagnation pressure, jet Mach number and jet mass flow rate is given. Using Equations (2.5), (2.8) and (2.9) required parameters are calculated. Jet inputs are given in Table A-2

Table A-2: TM-1-BT Jet boundary Conditions

M_{jet}	$\dot{m}$[kg/s]	P_{0jet}[psi]	P_{0j}[Pa]	P_{sj}[Pa]	T_{0jet}[K]	T_{jet}(K)
1	0.17	500	3447379	1821187	257,96	214,97

Jet exit is sonic in all jet-on CFD simulations in this study. It is found in literature [33] that greater force amplifications are obtained when jet exit is sonic, more than when the jet exit is subsonic. Type of the exit nozzle and inlet flow pattern is out of the scope of this study.

All calculated results for TM-1-BC is given in Table A-3. K and X_{CPi} are calculated from Equations (3-1) and (3-2) and Table A-3. Jet force is calculated from Equation (2-10) and using parameters in Table A-1 and Table A-2. All forces and moments are non dimensionalized by Equation (2-11), by using model diameter and cross sectional area.

Table A-3: TM-1-BC Results

TM-1 BC				
Alpha[º]	C_{N-REST}	C_{Njet}	$C_{N-jet\ on}$	$C_{N-jet\ off}$
-12	-1,7972	-0,6188	-2,4161	-1,8114
-8	-1,2409	-0,6188	-1,8597	-1,1880
-4	-0,6738	-0,6188	-1,2926	-0,5879
0	-0,1061	-0,6188	-0,7250	0,0002
4	0,4820	-0,6188	-0,1368	0,5871
8	1,0456	-0,6188	0,4267	1,1872
12	1,6489	-0,6188	1,0301	1,8120
Alpha[º]	$C_{m\|mc}$	$C_{m-jet\ off}$	**K**	X_{CPi}
-12	-0,4708	0,1236	0,977	0,983
-8	-0,4336	0,0708	1,085	0,751
-4	-0,3913	0,0330	1,139	0,602
0	-0,4053	0,0006	1,172	0,560
4	-0,4440	-0,0315	1,170	0,570
8	-0,4535	-0,0696	1,229	0,505
12	-0,4615	-0,1232	1,264	0,433